We thank the two reviewers for carefully reading our manuscript and for the important suggestions to improve it. Below we give detailed responses to all questions and comments from both reviewers. Reviewer comments are in red and start with **"R:"** and our replies are in black and start with **"A:"**. Original manuscript text is shown in blue, with new text highlighted in yellow.

With this response, we are also attaching 1) an annotated version of the manuscript indicating all changes; and 2) the updated manuscript.

=====================================
Reply to Reviewer #1

R: (1) Statistical significance still doesn't quite appear to be assessed correctly. The text is still vague on this, but it appears that the authors are only checking if the means +/- the standard errors overlap. Just because the errors bars do not overlap, does not mean the difference is significant. An actual statistical test (e.g. 2 sample t-test) needs to be used to assess differences. For example, in Table 3 for "All Layers" the lidar ratio differences are not statistically significant at 95% confidence (p=0.16). The authors should revisit the statistical test used and/or better explain what is being done in the text.

A: We apologize for not making this clearer in the text, but the statistical test we performed was actually a two-sample t-test between the two independent data sets (wet and dry) and not just comparing if means +/- the standard errors overlap as the Reviewer thought. Fortunately, the reviewer found the only typo in the table. The correct value for the lidar ratio in the dry season considering all layers is 24.4 sr and not 22.4 sr, as it was written. The typo probably occurred when we were transcribing the data from Matlab into the Word table.

We fixed this typo in the table and reviewed all other values. We could provide t-scores of this comparison by adding a new column in the table, but we felt that this would further pollute the table and would not bring relevant information. Nonetheless, for the reviewer benefit, we included t-scores in the two tables attached to this response. Please note that because of the high number of degrees of freedom, a 95% confidence is already found for t > 1.645. The new captions for tables 2 and 3 are:

Table 2. Summary of column-integrated statistics for the total time of observation, as well as for the wet, transition and dry seasons. Frequency of occurrence is calculated using a conditional sampling to avoid biases (session 2.4). Mean cirrus cloud properties and standard deviation of the sample (in parenthesis) are shown. The standard deviations of the mean were calculated and used to determine if seasonal differences (wet-dry) of the mean values are statistically significant to the 95% confidence level (indicated as *) using a 2-sample t-test. Geometrical properties are not given because most cloud profiles have more than one layer of cirrus. Lidar ratio is calculated as a column average.

Table 3. Summary of layer-statistics for the total time of observation, as well as for the wet, transition and dry seasons. Mean cirrus cloud properties and standard deviation of the sample (in parenthesis) are shown. The standard deviations of the mean were calculated and used to determine if seasonal differences (wet-dry) are statistically significant to the 95% confidence level (indicated as *) using a 2-sample t-test. Lidar ratio is calculated as a column average.

R: (2) I commend the authors for undertaking a full treating of multiple scattering. But, it is not clear how exactly the authors performed the correction. In the text, the authors simply state that they "perform a full treatment of multiple scattering following the model of Hogan (2008)". But the Hogan model is a forward model: i.e. it requires inputs of the true (single scattering) backscatter/extinction and from that computes the

measured (single and multiple scattering) signal. Therefore, what is retrieved from the lidar cannot be directly inputted into the Hogan model to get the multiple scattering effects. I suggest that the authors elaborate more on how they correct for multiple scattering.

In fact, the Hogan model is a forward model and thus the multiple scatter correction is done iteratively until the simulated multiple-scattered signal by Hogan's model converges to the true signal measured with the lidar. In the original Hogan model paper (Hogan, 2006 APPLIED OPTICS) he says that the purpose of the model is to be accurate and fast enough to be used iteratively and be used in a variational retrieval approach. Delanoe and Hogan (2008 JGR) have exemplified in detail this iterative process for ice clouds using the Hogan model, but this iterative method solution has already been used previously using Monte Carlo calculations of the effects of multiple scattering (e.g., Reichardt, 2006 APPLIED OPTICS)

The correction is done using a parameterization of ice crystals effective radius and the uncorrected extinction coefficient profile (iteration 0) to simulate a first SS/MS correction. This first correction is then applied to the original lidar profile and then we recalculate the extinction coefficient profile with the first correction (iteration 1). We re-run the model with the first correction of the extinction coefficient and the result calculated by the model is closer to the original lidar signal. We repeat this process (iteration 2,3,4 ...) until the signal calculated by the model converges to the original signal measured by the lidar. In general, with 2 or 3 iterations the result is already close to the corrected value, but we iterate 5 times. This iterative process was applied in all our profiles, which took a considerable computational time, even being the Hogan model accurate and fast.

To make this information clearer, the paragraph has been modified and now it is:

(...) For this reason, we refrain from applying empirical correction formulas (e.g. such as eq. 10 in Chen et al., 2002), and we instead perform a full treatment of multiple scattering following the model of Hogan (2008) that was used by. The correction is found iteratively, similar to Seifert et al. (2007) and Kienast-Sjögren et al. (2016). The forward model is initialized with the originally retrieved, uncorrected extinction profile, and the model output is used to correct the extinction profile iteratively, until it converges. In our case, we assumed the effective radius of ice crystals to vary with temperature according to a climatology of aircraft measurements of tropical cirrus data (Krämer et al., 2016a, 2016b), which includes the recent ACRIDICON field campaign with the German aircraft HALO in the Amazon region (Wendisch et al., 2016). The full treatment (...)

================================
Reply to Reviewer #2

We would like to thank reviewer # 2 J. Campbell for his comments, editing recommendations and questions. All of his textual corrections were accepted and corrected in the manuscript. Below are the replies to the other comments.

R: L. 123 – Consecutive?

A: Yes, consecutive. We do 1-min data acquisition. For this paper, however, each profile is the result of a continuous 5 min acquisition (i.e. time average), which represents 3000 laser shots at the repetition rate of 10Hz of our laser (a Quantel CFR-400).

We have modified the text to make this clear:

The lidar dataset used in the present study comprises measurements recorded between July 2011 and June 2012, which were temporally averaged into 5-min profiles (3000 laser shoots at 10 Hz). A total of 36,597 profiles were analyzed, corresponding roughly to 1/3 of the maximum possible number of profiles during 1 year.

R: L. 228 – Worries me slightly, but small concern. May want to check out Heymsfield et al, 2014 (JAS) to see how they compare?

A: I first came across the work of Heymsfield et al, 2014 (H14) through Campbell et al, 2016-JAMC and Lolli et al, 2016-ACPD. For temperatures below -60° C (usually> 12.5 km for our region) the parameterization of the effective radius of H14 and that provided by Kramer et al., 2016ab (K16) in tropical regions are very close, with a mean effective radius between 10 and 30 μm. For temperatures higher than -50°C, H14 correlates better with the K16 result for mid-latitudes (also with Wang and Sassen, 2002 in min-Lat.), which is on average larger when compared to tropical regions. Because the work of K16 also included very recent measurements in the Amazon region in 2014 (field campaign with German aircraft, HALO, for an overview see Wendisch et al. BAMS, January 2016), we chose to use K16.

We have modified the text to include the reference to the HALO campaign in the Amazon, and also to clarify to reviewer #1 how we did the multiple-scattering correction:

(…) For this reason, we refrain from applying empirical correction formulas (e.g. such as eq. 10 in Chen et al., 2002), and we instead perform a full treatment of multiple scattering following the model of Hogan (2008) that was used by. The correction is found iteratively, similar to Seifert et al. (2007) and Kienast-Sjögren et al. (2016). The forward model is initialized with the originally retrieved, uncorrected extinction profile, and the model output is used to correct the extinction profile iteratively, until it converges. In our case, we assumed the effective radius of ice crystals to vary with temperature according to a climatology of aircraft measurements of tropical cirrus data (Krämer et al., 2016a, 2016b), which includes the recent ACRIDICON field campaign with the German aircraft HALO in the Amazon region (Wendisch et al., 2016). The full treatment (…)

R: L. 306 – Average? Wow, that is high! Frequency absolute or relative?

A: When we speak of frequency of occurrence we are referring to the best estimate of the true frequency at which cirrus clouds are present over the measurement site, and is calculated considering all possible problems related to the extinction of the laser pulses by low clouds or other acquisition problems (as discussed in the new section 2.4, where we explain the conditional sampling proposed by Thorsen et al (2011) and Protat et al. (2014)). To keep the information complete, we also reported the number of profiles attenuated by low clouds or by something else at low levels (.i.e. and hence not used) in Table 2. This was also mentioned in this section.

R: L. 313 – repeated?

A: No. In the first paragraph we were considering the average value of this property when considering the entire column (integrated), which can contain several distinct clouds layers at the same time (data presented in table 2, where we also inform the average number of layers observed). This is interesting for possible comparison with non-profiling instruments (like sun photometers), because these will measure, for example, the optical depth of the whole integrated column.

The second paragraph is when we start to consider the properties of each cloud layer separately. As described in the text, distinct layers are considered when there is at least a column of 500 m of cloud-free air between them. The mean values for these distinct layers are shown in table 3.

To avoid this confusion, we rewrite the paragraph and make that clearer. Now it reads:

Table 2 shows column-integrated statistics of the properties of cirrus clouds during the one-year observational period, also divided for the different distinguished by season. On average, 1.4 layers of cirrus are present in each cloudy profile (1.25 during the dry, and 1.62 during the wet season). Column-integrated COD varies from 0.25 ± 0.45 in the dry season to 0.47 ± 0.65 in the wet season. The frequency of occurrence of opaque, thin and SVC column-integrated COD is 11.8 % (31.3 %), 23.9 % (37.9 %) and 23.3 % (18.3 %) respectively in the dry (wet) season. The maximum backscattering altitude does not show a seasonal cycle, and is on average 13.4 ± 2.0 km (or -60 ± 15 ^{o}C). The average number of simultaneous layers of cirrus present in each cloudy profile is 1.4 (1.25 during the dry, and 1.62 during the wet season), and hence geometrical properties, in a column-integrated sense, are not discussed.
As cirrus at different altitudes might have different origins or microphysical properties, it is more important to analyze the statistics based on each layer detected, as shown in Table 3. The overall mean value for the cloud layer base altitude is 12.9 ± 2.2 km, for the cloud layer top altitude, 14.3 ± 1.9 km, and for the cloud layer geometrical thickness, 1.4 ± 1.1 km. The mean value of the cloud layer maximum backscattering altitude is 13.6 ± 2.0 km. (…)

R: L. 346 – What about TTL Cirrus?

From our observations alone we cannot rule out that layers observed above the tropopause are not TTL cirrus. These can either be formed "*from ice detrainment from convective towers or from in situ formation in supersaturated regions created by large- to mesoscale uplifts*" (e.g. Wang and Dessler, 2012). Garret et al. (2004) mention that these thin tropopause cirrus "*originate as stratiform pileus clouds that form near the tropopause ahead of vigorous convective uplift".* They then "*hypothesize that the pileus are penetrated by the convection, moistened through turbulent mixing, and once the convection subsides, they are sustained by radiative cooling due to the presence of the anvil layer beneath".* It should be noted, however, that until nowadays "*the respective importance of homogenous and heterogeneous nucleation remains unclear, although in situ observations suggest that both are active in the TTL" (Jensen et al., 2013; Cziczo et al., 2013).* Finally, it is still unknown the "*role of different waves with different scales on cirrus processes"* (Kim and Alexander, 2015).

Because of this difficulty, we have until now refrained from talking about TTL, although we suspect that the thin cirrus we observed above the tropopause base are exactly that. We have mentioned convection overshooting and detrainment, which we could observe (or infer), but not about the possible in-situ formation. We note, however, that the necessary large-scale uplifts in the Amazon are easily found around mesoscale convective systems (MCS), which are very common feature of the Amazon hydrological cycle. Figure below gives an example of thin TTL cirrus that appears to be over an anvil cloud:

We agree with the reviewer that mentioning TTL cirrus would be important. We did not include the picture, but we changed the text around line 346 as follows:

Moreover, while the distribution of opaque cirrus peaks at 12 km height in both seasons, thin cirrus and SVC shows a bimodal distribution only in the wet season, with the highest maxima above 14 km and 16 km respectively. This is presumably associated with the overshooting convection discussed above, which occurs mostly during the wet season (Liu and Zipser, 2005). Moreover, ice detrainment directly into the tropical tropopause layer (TTL) is one of the main mechanisms of TTL cirrus formation; the other is in-situ formation by supersaturation promoted by mesoscale uplift (Cziczo et al., 2013), which

can occur above tropical convective systems (Garret et al., 2004), a very common feature of the Amazon hydrological cycle.

The conclusion was changed as well:

The geometrical, and optical, and mycrophysical characteristics of cirrus clouds measured in the present study were consistent with other reports from tropical regions. The mean values were 12.9 ± 2.2 km (base), 14.3 ± 1.9 km (top), 1.4 ± 1.1 km (thickness), and 0.25 ± 0.46 (optical depth). Cirrus clouds were found at temperatures down to −90 °C and maximum backscatter altitude was 13.6 ± 2.0. 6 % (16 %) of the observed cirrus had their base (top) above the tropopause level or in the tropical tropopause layer.

By simultaneously analyzing cloud altitude and COD, it was found that cirrus clouds observed during the dry season months are optically thinner and lower in altitude than those during the wet period. The vertical distribution of frequency of occurrence is mono-modal, and 13 % of the observed cirrus had top within the TTL. During the wet season months, there is a wider range of COD for a fixed altitude, and vice-versa, which is associated with the variability in the intensity of deep convection in Amazonia. The vertical distribution of the frequency of occurrence of the detected clouds shows a bimodal distribution for thin and SV cirrus, and 19 % of the observed cirrus had top within the TTL, which are likely associated to slow mesoscale uplifting or to the remnants of overshooting convection.

And the abstract:

(…) The mean values of cirrus cloud top and base heights, cloud thickness and cloud optical depth were 14.3 ± 1.9 (std) km, 12.9 ± 2.2 km, 1.4 ± 1.1 km, and 0.25 ± 0.46, respectively. Cirrus clouds were found at temperatures down to −90 °C. 6 % of the Cirrus clouds were above the base of the tropical tropopause layer. Frequently cirrus were observed within the TTL, which are likely associated to slow mesoscale uplifting or to the remnants of overshooting convection. The vertical (…)

These are the references we mentioned:

Cziczo, D. J., Froyd, K. D., Hoose, C., Jensen, E. J., Diao, M., Zondlo, M. A., Smith, J. B., Twohy, C. H., and Murphy, D. M.: Clarifying the dominant sources and mechanisms of cirrus cloud formation., Science, 340, 1320–1324, doi:10.1126/science.1234145, 2013.

Garrett, T. J., A. J. Heymsfield, M. J. McGill, B. A. Ridley, D. G. Baumgardner, T. P. Bui, and C. R. Webster (2004), Convective generation of cirrus near the tropopause, J. Geophys. Res., 109, D21203, doi:10.1029/2004JD004952.

Jensen, E. J., Diskin, G., Lawson, R. P., Lance, S., Bui, T. P., Hlavka, D., McGill, M., Pfister, L., Toon, O. B., and Gao, R.: Ice nucleation and dehydration in the Tropical Tropopause Layer, P. Natl. Acad. Sci. USA, 110, 2041–2046, doi:10.1073/pnas.1217104110, 2013.

Kim, J.-E. and Alexander, M. J.: Direct impacts of waves on tropical cold point tropopause temperature, Geophys. Res. Lett., 42, 1584–1592, doi:10.1002/2014GL062737, 2015.

Wang, T. and Dessler, A. E.: Analysis of cirrus in the tropical tropopause layer from CALIPSO and MLS data: A water perspective, J. Geophys. Res.-Atmos., 117, 2156–2202, doi:10.1029/2011JD016442, 2012

R: L. 377 – Define "last for a long time"

A: We have modified the text as follows.

These cirrus that has formed around the tropopause cannot last for long time (typically less than a day; Jensen et al., 1996), as they cannot be adiabatically lifted above the tropopause inversion (Jensen et al., 1996).

R: L. 382 – Right … in Campbell et al, (2016) we saw a similar distribution, which we thought was skewed by sample bias.

A: Ok.

R: L. 397 – Nice! If you are interest look at JTECH Early online release for new paper by our group from Marquis et al …

A: Very interesting, thanks for pointing out this reference.

Table 2. Summary of column-integrated statistics for the total time of observation, as well as for the wet, transition and dry seasons. Frequency of occurrence is calculated using a conditional sampling to avoid biases (session 2.4). Mean cirrus cloud properties and standard deviation of the sample (in parenthesis) are shown. The standard deviations of the mean were calculated and used to determine if seasonal differences (wet-dry) of the mean values are statistically significant to the 95% confidence level (indicated as *) using a 2-sample t-test. Geometrical properties are not given because most cloud profiles have more than one layer of cirrus. Lidar ratio is calculated as a column average.

	Total	Wet	Transition	Dry	tstat
Observation time [%] [a]	37.4	41.5	21.9	48.9	
N. prof. measured [b]	36844	13828	7423	15593	
N. prof. used in analysis [c]	16025	3458	2099	10468	
N. prof. discarded for apparent top [d]	476	223	148	105	
Frequency of Occurrence [%]*	73.8	88.1	74.2	59.2	40.5
N. prof. w/ cirrus	11252	3145	1706	6397	
Frequency of Occurrence, Opaque [%]*	22.6	31.3	24.6	11.8	25.0
N. prof. w/ cirrus, Opaque	3327	1316	610	1401	
Frequency of Occurrence, Thin [%]*	32.8	37.9	36.5	23.9	14.8
N. prof. w/ cirrus, Thin	4577	1224	798	2555	
Frequency of Occurrence, SVC [%]*	18.3	18.7	13.0	23.3	5.8
N. prof. w/ cirrus, SVC	3322	603	296	2423	
Cloud Optical Depth*	0.35 (0.55)	0.47 (0.65)	0.40 (0.57)	0.25 (0.45)	16.8
Max Backscatter Altitude [km]*	13.4 (2.0)	13.4 (2.2)	13.3 (2.2)	13.6 (1.7)	-4.9
Temperature Max. Back. Alt. [°C]*	-60 (15)	-60 (16)	-59 (17)	-62 (13)	5.4
Lidar Ratio [sr]* [e]	23.6 (8.1)	22.8 (8.0)	22.8 (7.8)	24.6 (7.7)	-9.3
Num. of cirrus layers per cloud prof.	1.41 (0.63)	1.62 (0.77)	1.61 (0.67)	1.25 (0.48)	

[a] Fraction of observation time to total possible time (21h per day)
[b] Total number of profiles measured, i.e. not screened for low clouds or precipitation
[c] Refers to the number of 5-min profiles with high enough SNR (section 2.4)
[d] Number of profiles with apparent cirrus top, considering only good profiles
[e] All layers in the same profile share the same average LR

Table 3. Summary of layer-statistics for the total time of observation, as well as for the wet, transition and dry seasons. Mean cirrus cloud properties and standard deviation of the sample (in parenthesis) are shown. The standard deviations of the mean were calculated and used to determine if seasonal differences (wet-dry) are statistically significant to the 95% confidence level (indicated as *) using a 2-sample t-test. Lidar ratio is calculated as a column average.

	Total	Wet	Transition	Dry	tstat
All Layers					
Num. of cirrus layers	15824	5096	2739	7989	
Base Altitude [km]*	12.9 (2.2)	12.8 (2.4)	12.6 (2.3)	13.0 (1.9)	-4.7
Top Altitude [km]	14.3 (1.9)	14.3 (2.0)	14.1 (2.0)	14.3 (1.6)	0.8
Thickness [km]*	1.4 (1.1)	1.5 (1.2)	1.5 (1.1)	1.3 (1.0)	11.0
Cloud Optical Depth*	0.25 (0.46)	0.30 (0.52)	0.26 (0.47)	0.20 (0.40)	11.6
Max Backscatter Altitude [km]	13.6 (2.0)	13.7 (2.3)	13.5 (2.2)	13.6 (1.8)	1.0
Lidar Ratio [sr]*	23.3 (8.0)	22.6 (8.1)	22.8 (7.9)	24.4 (7.9)	-11.3
Relative freq. opaque cirrus [%]*	20.5	25.2	21.0	17.4	10.5
Relative freq. thin cirrus [%]	37.8	37.0	43.2	36.5	0.6
Relative freq. SVC [%]*	41.6	37.8	35.8	46.0	9.2
Base above the tropopause [%]*	5.9	6.9	5.5	5.3	3.8
Top above the tropopause [%]*	15.7	18.7	16.1	12.9	8.7
Opaque Layers					
Num. of opaque layers	3251	1283	574	1394	
Base Altitude [km]*	10.7 (1.5)	10.6 (1.6)	10.4 (1.5)	10.8 (1.2)	-3.5
Top Altitude [km]	13.4 (1.6)	13.5 (1.7)	13.1 (1.6)	13.6 (1.4)	-1.4
Thickness [km]*	2.76 (1.02)	2.84 (1.07)	2.65 (1.04)	2.73 (0.94)	2.8
Cloud Optical Depth*	0.93 (0.64)	1.00 (0.66)	0.90 (0.66)	0.86 (0.59)	5.5
Max Backscatter Altitude [km]	12.0 (1.7)	12.1 (1.9)	11.6 (1.7)	12.1 (1.5)	-0.7
Lidar Ratio [sr]*	25.7 (6.3)	26.0 (6.7)	25.8 (6.6)	25.3 (5.7)	3.1
Thin Layers					
Num. of thin layers	5985	1888	1183	2914	
Base Altitude [km]*	12.9 (1.7)	13.1 (1.9)	12.9 (1.8)	12.8 (1.4)	6.8
Top Altitude [km]*	14.4 (1.7)	14.6 (2.0)	14.4 (1.8)	14.3 (1.4)	5.8
Thickness [km]*	1.46 (0.78)	1.42 (0.82)	1.49 (0.78)	1.47 (0.74)	-2.0
Cloud Optical Depth	0.12 (0.07)	0.12 (0.07)	0.12 (0.07)	0.11 (0.07)	1.2
Max Backscatter Altitude [km]*	13.7 (1.7)	13.9 (1.9)	13.7 (1.9)	13.5 (1.5)	7.0
Lidar Ratio [sr]*	22.8 (7.9)	21.8 (7.7)	21.6 (7.4)	24.3 (8.1)	-11.0
SVC Layers					
Num. of SVC layers	6581	1924	980	3677	
Base Altitude [km]*	14.4 (1.9)	14.7 (2.1)	14.4 (2.1)	14.2 (1.6)	8.4
Top Altitude [km]*	14.9 (1.9)	15.2 (2.1)	15.0 (2.1)	14.7 (1.6)	8.4
Thickness [km]	0.51 (0.37)	0.50 (0.38)	0.53 (0.38)	0.51 (0.36)	-0.7
Cloud Optical Depth	0.011 (0.008)	0.011 (0.008)	0.012 (0.009)	0.011 (0.008)	1.6
Max Backscatter Altitude [km]*	14.6 (1.9)	14.9 (2.1)	14.7 (2.1)	14.4 (1.6)	8.7
Lidar Ratio [sr]*	21.6 (8.4)	19.9 (7.6)	21.5 (8.1)	23.5 (9.0)	-10.8

1 **Optical and Geometrical Properties of Cirrus Clouds in**
2 **Amazonia Derived From 1-year of Ground-based Lidar**
3 **Measurements**
4

5 Diego A. Gouveia[1], Boris Barja[1,2,3], Henrique M. J. Barbosa[1], Patric Seifert[4], Holger
6 Baars[4], Theotonio Pauliquevis[5], and Paulo Artaxo[1].

7 [1]Applied Physics Department. Institute of Physics, University of São Paulo, São Paulo, SP, Brazil.

8 [2]Atmospheric Optics Group of Camagüey. Meteorological Institute of Cuba, Cuba.

9 [3]Atmospheric Research Laboratory, University of Magallanes, Punta Arenas, Chile.

10 [4]Leibniz Institute for Tropospheric Research (TROPOS), Leipzig, Germany

11 [5]Department of Environmental Sciences, Federal University of São Paulo, Diadema, SP, Brazil.

12

13 *Correspondence to:* Boris Barja Gonzalez (bbarja@gmail.com)

14 **Abstract.** Cirrus clouds cover a large fraction of tropical latitudes and play an important role in Earth's
15 radiation budget. Their optical properties, altitude, vertical and horizontal coverage control their radiative
16 forcing, and hence detailed cirrus measurements at different geographical locations are of utmost
17 importance. Studies reporting cirrus properties over tropical rain forests like the Amazon, however, are
18 scarce. Studies with satellite profilers do not give information on the diurnal cycle, and the satellite
19 imagers do not report on the cloud vertical structure. At the same time, ground-based lidar studies are
20 restricted to a few case studies. In this paper, we derive the first comprehensive statistics of optical and
21 geometrical properties of upper-tropospheric cirrus clouds in Amazonia. We used one year (July 2011 to
22 June 2012) of ground-based lidar atmospheric observations north of Manaus, Brazil. This dataset was
23 processed by an automatic cloud detection and optical properties retrieval algorithm. Upper-tropospheric
24 cirrus clouds were observed more frequently than reported previously for tropical regions. The frequency
25 of occurrence was found to be as high as 88 % during the wet season and not lower than 50 % during the
26 dry season. The diurnal cycle shows a minimum around local noon and maximum during late afternoon,
27 associated with the diurnal cycle of precipitation. The mean values of cirrus cloud top and base heights,
28 cloud thickness and cloud optical depth were 14.3 ± 1.9 (std) km, 12.9 ± 2.2 km, 1.4 ± 1.1 km, and
29 0.25 ± 0.46, respectively. Cirrus clouds were found at temperatures down to -90 °C. Frequently cirrus
30 were observed within the TTL, which are likely associated to slow mesoscale uplifting or to the remnants
31 of overshooting convection. The vertical distribution was not uniform, and thin and subvisible cirrus
32 occurred more frequently closer to the tropopause. The mean lidar ratio was 23.3 ± 8.0 sr. However, for
33 subvisible cirrus clouds a bimodal distribution with a secondary peak at about 44 sr was found suggesting
34 a mixed composition. A dependence of the lidar ratio with cloud temperature (altitude) was not found,
35 indicating that the clouds are vertically well mixed. The frequency of occurrence of cirrus clouds

Henrique de Melo Jorg…, 7/2/2017 15:54
Deleted: 6 % of the Cirrus clouds were above the base of the tropical tropopause layer.

classified as subvisible ($\tau < 0.03$) were 41.6 %, whilst 37.8 % were thin cirrus ($0.03 < \tau < 0.3$) and 20.5 % opaque cirrus ($\tau > 0.3$). Hence, in central Amazonia not only a high frequency of cirrus clouds occurs, but also a large fraction of subvisible cirrus clouds. This high frequency of subvisible cirrus clouds may contaminate aerosol optical depth measured by sun-photometers and satellite sensors to an unknown extent.

1. Introduction

Clouds cover on average about 50 % of the Earth's surface (Mace et al., 2007) and cirrus alone cover 16.7 % (Sassen et al., 2008), with higher fractions occurring in the Tropics (Sassen et al., 2009). Hence cirrus are important to understand current climate and to predict future climate (Wylie et al. 2005, Stubenrauch et al. 2006; Nazaryan et al., 2008). Several studies emphasize the important role that cirrus clouds play in the Earth's radiation budget (i.e. Liou 1986; Lynch et al. 2002; Yang et al. 2010a). Their role is twofold. First, cirrus clouds increase warming by trapping a portion of infrared radiation emitted by the Earth/atmosphere system. Second, cirrus clouds cool the atmosphere by reflecting part of the incoming solar radiation back into space. The contribution of each effect and the net effect on the radiative forcing depends strongly on cirrus cloud optical properties, altitude, vertical and horizontal coverage (Liou 1986, Kienast-Sjögren et al. 2016). Therefore, understanding their properties is critical to determining their impact on planetary albedo and greenhouse effects (Barja and Antuña, 2011, Boucher et al., 2013). Also, tropical cirrus clouds could influence the vertical distribution of radiative heating in the tropical tropopause layer (e.g., Yang et al., 2010b; Lin et al., 2013). Noticeably, it has been shown that an accurate representation of cirrus vertical structure in cloud radiative studies improves the results of these calculations (Khvorostyanov and Sassen, 2002; Hogan and Kew, 2005; Barja and Antuña, 2011). Recent research also shows that an increase of stratospheric water vapor is linked mainly to the occurrence of cirrus clouds in the tropical tropopause layer (TTL) (Randel and Jensen, 2013). Finally, measurements of the properties of cirrus clouds at different geographical locations are of utmost importance, potentially allowing for improvements in numerical model parameterizations and, thus, reducing the uncertainties in climatic studies.

Ground-based lidars are an indispensable tool for monitoring cirrus clouds, particularly those cirrus clouds with very low optical depth, which are undetectable for cloud radars (Comstock et al., 2002) or for passive instruments (e.g., Ackerman et al., 2008). For this reason, several studies with ground-based lidars have reported the characteristics of cirrus clouds around the globe during the last decade. There are some long-term studies reporting climatologies at midlatitudes (eg. Sassen and Campbell, 2001; Goldfarb et al., 2001; Giannakaki et al., 2007; Hoareau et al., 2013; Kienast-Sjögren et al. 2016) and tropical regions (eg. Comstock et al., 2002; Cadet et al., 2003; Antuña and Barja, 2006; Seifert et al., 2007; Thorsen et al., 2011; Pandit et al., 2015). Table 1 shows an overview of these studies with different values for cirrus clouds characteristics in diverse geographical regions. There are also some short-term reports on cirrus clouds characteristics during measurement campaigns at midlatitudes (e.g. Immler and Schrems, 2002a) and tropical latitudes (Immler and Schrems, 2002b, Pace et al., 2003 and references therein). Additionally, satellite-based lidar measurements have been used to investigate the global distribution of cirrus characteristics (eg. Nazaryan et al., 2008; Sassen et al., 2009; Sassen et al., 2009; Wang and

2

Dessler 2012, Jian et al., 2015). Characteristics of tropical and subtropical cirrus clouds have similar geometrical values and they occur at higher altitudes than those at midlatitudes. However, the frequencies of occurrence of cirrus cloud types differ significantly between different locations.

Reports on cirrus cloud measurement over tropical rain forests like in Amazonia are scarce. Just a few global studies with satellite instruments include these regions, and they do not provide information on the diurnal cycle. There are also a few studies focused on deep convection in Amazonia that report cirrus clouds (eg. Machado et al., 2002; Hong et al., 2005; Wendisch et al., 2016), but no lidar measurements were used. Baars et al. (2012) focused on aerosol observations with a ground-based Raman lidar, and thus report only one cirrus cloud case that was observed between 12 km and 16 km height on 11 September 2008 during an 11-month measurement period in 2008. Barbosa et al. (2014) describe a week of cirrus cloud measurements performed from 30 August to 6 September 2011 during an intensive campaign for calibration of the water vapor channel of the UV Raman lidar, which is also used in this study. Cirrus clouds during that period were present in 60% of the measurements. Average base and top heights were 11.5 km and 13.4 km, respectively, and average maximum backscatter occurred at 12.8 km. Most of the time, two layers of cirrus clouds were present.

From the above discussion, the importance of continuous and long-term observations of tropical cirrus clouds is evident. In the present study, we use one year of ground-based lidar measurements (July 2011 to June 2012) at Manaus, Brazil to investigate the seasonal and daily cycles of geometrical (cloud top and base altitude) and optical (cloud optical depth and lidar ratio) properties of cirrus over a tropical rain forest site. In section 2, a description of the Raman lidar system, dataset, processing algorithms and site are given. The results and discussion are presented in section 3. We close this paper with concluding remarks in section 4.

2. Instrumentation, dataset and algorithms.

2.1. Site and instrument description

The ACONVEX (Aerosols, Clouds, cONVection EXperiment) or T0e (nomenclature of the GoAmazon2014/15 experiment, Martin et al. 2016) site is located up-wind from Manaus-AM, Brazil, at 2.89° S and 59.97° W, in the central part of the Amazon Forest, as shown in the satellite image of Figure 1. Atmospheric observations at this site began in 2011 with the objective to operate a combination of several instruments for measuring atmospheric humidity, clouds and aerosols as well as processes which lead to convective precipitation (Barbosa et al., 2014).

As with most tropical continental sites, the diurnal cycle of precipitation is strong with a late afternoon peak (Adams et al., 2013). The precise definition of the climatological seasons varies among authors (e.g. Machado et al., 2004, Arraut et al., 2012, Tanaka et al., 2014), however, deep convection is a characteristic of the region all year. For our site and period of study, we considered a wet (Jan-Apr), dry (Jun-Sep), and transition (Mar, Oct-Dec) season respectively. Convection is more active during the wet season, when the intertropical convergence zone (ITCZ) influences the region. As the ITCZ moves northward during the months of the dry month, convective activity decreases.

3

The lidar system (LR-102-U-400/HP, manufactured by Raymetrics Advanced Lidar Systems) operates in the ultraviolet (UV) at 355 nm. Three channels detect the elastically backscattered light at 355 nm as well as the Raman-scattered light of nitrogen (387 nm) and water vapor (408 nm), simultaneously in analog and photon-counting modes. The system is tilted by 5° from the zenith to avoid specular reflection of horizontally-oriented ice crystals (e.g., Westbrook et al., 2010). It is automatically operated 7 days a week, only being closed between 11 am and 2 pm local time (LT is −4 UTC) to avoid the sun crossing the field of view. Detailed information about the lidar system and its characterization are given by Barbosa et al. (2014). To retrieve the particle backscatter and extinction profiles from the lidar signal, the temperature and pressure profiles were obtained from radio soundings launched at 0 and 12 UTC from the Ponta Pelada Airport, located 28.5 km to the South (3.14°S, 59.98°W) of the experimental site.

2.2. Datasets

The lidar dataset used in the present study comprises measurements recorded between July 2011 and June 2012, which were temporally averaged into 5-min profiles (3000 laser shoots at 10 Hz). A total of 36,597 profiles were analyzed, corresponding roughly to 1/3 of the maximum possible number of profiles during 1 year.

For the long-term analysis, winds were obtained from the ERA Interim reanalysis (Dee et al., 2011) of European Center for Midrange Weather Forecast (ECMWF) with spatial resolution of 0.75° and temporal resolution of 6 h. The tropopause altitudes were calculated using ERA Interim temperature profiles interpolated to the measurement time of each cirrus layer observation. We followed the definition of the World Meteorological Organization (IMV WMO, 1966), i.e. *"the lowest level at which the lapse rate decreases to 2 °C km^{-1} or less, provided that the average lapse rate between this level and all higher levels within 2 km does not exceed 2 °C km^{-1}"*. We further assumed the lapse rate to vary linearly with pressure (McCalla, 1981), and the exact altitude where Γ=2 °C km^{-1} (i.e. the tropopause) was found by linearly interpolating between the closest available pressure levels. Precipitation was obtained from TRMM (Tropical Rainfall Measuring Mission) version 7 product 3B42 (Huffman et al., 2007) with 0.25° and 3 h of spatial and temporal resolution, respectively. Back trajectories were calculated using the HYSPLIT model (Stein et al., 2015) forced by meteorological fields from the US National Oceanic and Atmospheric Administration (NOAA) Global Data Assimilation System (GDAS), available at 0.5 degree resolution.

2.3. Cirrus cloud detection algorithm.

We used an automatic algorithm for the detection of the cloud base, the cloud top and the maximum backscattering heights, based on Barja and Aroche (2001). The algorithm is explained in detail in Barbosa et al. (2014) and is in here only described briefly. Basically, it assumes a monotonically decreasing intensity of the lidar signal with altitude in a clear atmosphere and searches for significant abrupt changes. These abrupt changes are marked as a possible cloud base. Examining the signal noise, each true cloud base is discriminated. Then, the lowest altitude above cloud base with signal lower than that at cloud base and corresponding to a molecular gaseous atmosphere is determined as the cloud top. When more than one layer is present in the same profile, and their top and base are separated more than 500 m, they are

171 considered as individual clouds. Figure S.2 gives an example of cloud detection. Barbosa et al. (2014)
172 also provide information on the discrimination of false positives and the distinguishing of aerosols from
173 thin cloud layers. After obtaining the base, top and maximum backscatter heights, the corresponding
174 cloud boundary temperatures are obtained from the nearest radiosonde. A detected high cloud is classified
175 as a cirrus cloud if the cloud top temperature is lower than $-37\ ^{\circ}$C (Sassen and Campbell, 2001; Campbell
176 et al., 2015). These temperatures are typically found at about 10.5 km height over Amazonia.

2.4. Frequency of Occurrence and Sampling Issues

178 In a simplified manner, the frequency of occurrence would just be the ratio of the number of profiles with
179 cirrus clouds to the total number of profiles. However, while one might be sure when a cirrus cloud was
180 detected in a given profile, there is no certainty of its presence when the profile has a low signal-to-noise
181 ratio or when there is no measurement available. Sampling cirrus clouds with a ground-based profiling
182 instrument can be problematic, particularly for the calculation of the temporal frequency of occurrence,
183 due to the obscuration by lower clouds, or availability of measurements, which might introduce sampling
184 biases (Thorsen et al., 2011).
185 To avoid these sampling issues, we use an approach similar to the conditional sampling proposed by
186 Thorsen et al. (2011) and Protat et al. (2014). First, we recognize that the presence of cirrus clouds is
187 rather independent of low-level liquid water clouds that can fully attenuate the laser beam, and
188 independent of instrumental issues that might restrict measurement time. Hence, the best estimate of the
189 true frequency of occurrence is the ratio of the number of profiles with cirrus, by the number of profiles
190 where cirrus could have been detected.
191 These qualifying profiles are identified as follows. The noise in each clear-sky bin follows a Poisson
192 distribution and is evaluated as the square root of the signal. The signal-to-noise ratio (SNR) is defined as
193 the background corrected signal divided by the noise, similar to Heese et al. (2010). Profiles are selected
194 if a clear-sky SNR higher than 1.0 is found at 16 km, for 7.5 m vertical resolution. Note that this is not the
195 SNR of the cirrus cloud (cirrus – molecular / noise), which typically ranges from 6 to 36. The threshold
196 was obtained from a performance evaluation of the detection algorithm. Using simulations, we varied
197 cloud thickness (15 m to 4.5 km), cloud backscatter coefficient (1 to 10 Mm^{-1} sr^{-1}) and SNR (1 to 50). We
198 found that our algorithm detects 99% of cirrus clouds with COD > 0.005. In other words, given typical
199 cirrus cloud optical depths, the threshold used implies a sufficiently high SNR at cloud top for applying
200 the transmittance method (described in section 2.5).
201 From analysis of the available profiles, 16,025 were found to satisfy these criteria (see Table 2). July,
202 August and September, the driest months, show the highest fraction of profiles with good SNR, while the
203 wettest months have the lowest fraction of lidar profiles with good SNR (see figure S.1). To avoid
204 introducing biases from the different sample sizes in different months, the frequency of occurrence for the
205 year is calculated as the average frequency of occurrence for each season. The frequency for each season,
206 in turn, is calculated from the frequency of each month. Finally, the frequency for each month is
207 calculated by averaging over the mean diurnal cycles (i.e. mean of hourly means), because there are more
208 profiles with good SNR during night compared to daytime.

2.5. Cloud Optical Depth, backscattering coefficient and lidar ratio

Attenuation of the lidar signal by cirrus clouds can be obtained using the ratio of the range-corrected signal at the top and at the cloud base as described in Young (1995):

$$\frac{S(z_t)}{S(z_b)} = \frac{\beta(z_t)}{\beta(z_b)} e^{-2\int_{z_b}^{z_t}\alpha_p(z')dz'} e^{-2\int_{z_b}^{z_t}\alpha_m(z')dz'} \quad , \tag{1}$$

where z_b and z_t are the base and top height of a cirrus layer, and $S(z) = P(z)z^2$ is the range corrected signal. $\beta(z)$ and $\alpha(z)$ are the volumetric backscattering and extinction coefficients, respectively, and each is the sum of a molecular (sub index m) and a particle (sub index p) contribution. Volumetric backscattering and extinction profiles from molecules were derived following Bucholtz (1995). Assuming a negligible aerosol contribution in the atmospheric layers just below and above the cirrus clouds (Young, 1995), we can express the transmittance factor of the lidar equation due to the cirrus layer, T^{cirrus}, as

$$T^{cirrus} = e^{-2\int_{z_b}^{z_t}\alpha_p(z')dz'} = \frac{S(z_t)}{S(z_b)}\frac{\beta(z_b)}{\beta(z_t)}e^{2\int_{z_b}^{z_t}\alpha_m(z')dz'} \quad , \tag{2}$$

and the cirrus optical depth (for an example, see Figure S.2), τ^{cirrus}, as

$$\tau^{cirrus} = \int_{z_b}^{z_t}\alpha_p(z')dz' = -\frac{1}{2}\ln(T^{cirrus}) \quad . \tag{3}$$

The accuracy of this calculation depends mainly on the SNR at the cirrus cloud altitude. However, when the lidar signal is completely attenuated by the cirrus cloud (i.e. the transmission factor approaches zero) it is impossible to obtain the true values of the cirrus top altitude and optical depth. The retrievals, in these cases called apparent values, are necessarily underestimated and were not included in our analysis (see Table 2).

The backscattering coefficients of cirrus clouds were determined by the Fernald-Klett-Sasano method (Fernald et al., 1972; Klett, 1981; Sasano and Nakane, 1984) for each 5-min averaged profile having cloud and satisfying the conditions discussed in the previous section. For retrieving extinction, the Klett method requires a predetermined value for the layer-mean lidar ratio (LR), which is the ratio between the extinction and backscattering coefficients. Then, integrating the extinction coefficient from the cloud base to cloud top, the cirrus cloud optical depth is obtained (τ_{Klett}^{cirrus}). Following Chen et al. (2002), we estimated the value of LR for every cloud profile by iterating over a range of values of LR and comparing the values of τ_{Klett}^{cirrus} with the independent value of the cirrus optical depth obtained from the transmittance method described above (τ^{cirrus}). The cirrus mean lidar ratio is the one that minimizes the residue: $R(S) = (\tau_{Klett}^{cirrus} - \tau^{cirrus})^2$. We use the approach of Chen et al. (2002) instead of the Raman method (Ansman et al., 2002) because our instrument can only detect the Raman scattered light at nitrogen during nighttime as Raman scattering is very weak compared to the elastic scattering. Moreover, the Raman results are very noisy even during nighttime and, by analyzing simulated lidar profiles (not shown), we found that for the given setup of our study (24/7 analysis of 5-min profiles) a more precise and accurate cirrus layer-mean LR can be obtained with the Chen et al. (2002) method.

The Klett method assumes single scattering, but eventually the received photons could have been scattered by other particles multiple times before reaching the telescope. This effect, named multiple scattering, increases the apparent laser transmittance and decreases the corresponding extinction coefficient values. Inversion of uncorrected signals could bias the extinction, and hence the COD and LR, typically by 5-30% (Thorsen and Fu, 2015). This is particularly important at UV wavelengths, for which a

Henrique de Melo Jorg…, 1/2/2017 11:35
Deleted: The a

Henrique de Melo Jorg…, 1/2/2017 11:36
Deleted: that have

Henrique de Melo Jorg…, 1/2/2017 11:36
Deleted: ied

Henrique de Melo Jorg…, 1/2/2017 11:36
Deleted: the

Henrique de Melo Jorg…, 1/2/2017 11:37
Deleted: 's

Henrique de Melo Jorg…, 1/2/2017 11:37
Deleted: real

much stronger forward scattering and therefore larger amounts of multiple scattering occur compared to the visible or infrared wavelengths. For this reason, we refrain from applying empirical correction formulas (e.g. such as eq. 10 in Chen et al., 2002), and instead perform a full treatment of multiple scattering following the model of Hogan (2008). The correction is found iteratively, similar to Seifert et al. (2007) and Kienast-Sjögren et al. (2016). The forward model is initialized with the originally retrieved, uncorrected extinction profile, and the model output is used to correct the extinction profile iteratively, until it converges. In our case, we assumed the effective radius of ice crystals to vary with temperature according to a climatology of aircraft measurements of tropical cirrus data (Krämer et al., 2016a, 2016b), which includes the recent ACRIDICON field campaign with the German aircraft HALO in the Amazon region (Wendisch et al., 2016). The full treatment corrects the retrieved LR by about 40%, from $16.8 \pm 5.8\ sr$ (uncorrected) to $23.6 \pm 8.1\ sr$, while Chen's approach would only correct it to $20.2 \pm 7.0\ sr$. In the following sections, all cirrus optical properties (lidar ratio, extinction coefficient, and optical depth) derived in the frame of this study were corrected for multiple-scattering.

3. Results and discussion.

3.1. Frequency of cirrus cloud occurrence.

A total of 11,252 lidar profiles were recorded with the presence of cirrus clouds, yielding an average temporal frequency of cirrus cloud occurrence of 73.8 % from July 2011 to June 2012. Figure 2 shows the monthly frequency of cirrus cloud occurrence, with statistical error, and precipitation in central Amazonia. There is a well-defined seasonal cycle, with maximum values from November to April, reaching 88.1 % during the wet season, and a minimum value in August during the dry season (59.2 %), but with frequencies not lower than 50 % (see Table 2). Moreover, the mean monthly cirrus cloud frequency follows the same seasonal cycle as accumulated precipitation, which responds to the seasonal changes of the ITCZ, and is higher from January to April and lower from June to September (Machado et al., 2002; 2014). Mean cirrus frequencies during the wet months are higher by a statistically significant amount than during dry months (notice the small standard deviation of the mean despite the high variability). This result and the lack of the other possible formation mechanisms proposed in the literature (Sassen et al., 2002) suggest that deep convection is the main formation mechanism for cirrus clouds in central Amazonia. Deep convective clouds generate cirrus clouds when winds in the upper troposphere remove ice crystals of the top of the large convective column, generating anvil clouds. Anvil clouds remain even after the deep convective cloud dissipates and persists from 0.5 to 3.0 days (Seifert et al, 2007).

To further investigate the role of deep convection as the main local formation mechanism, the high-altitude circulation and spatial distribution of precipitation were studied. The mean wind field at 150 hPa, approximately the mean cirrus top-cloud altitude (14.3 km, see Table 3), and accumulated precipitation are shown in Figure 3. The study period was divided into wet (January, February, March and April), dry (June, July, August and September) and transition (May, October, November and December) periods, based on accumulated precipitation. During the wet months, the South American monsoon is prevalent, and associated rain amounts range from 8 to 14 mm/day, with monthly totals of about 300 mm. Winds at

318 150 hPa blow from the southeast at about 6 m/s. During the dry period, convective activity moved to the
319 north toward Colombia and Venezuela and the 150 hPa air flow is from the west, also at about 6 m/s, thus
320 allowing cirrus clouds to be advected by 520 km or 4.5^o per day. As previous studies reported that
321 tropical cirrus could be transported by thousands of kilometers (e.g. Fortuin et al., 2007), 24-h back-
322 trajectories were calculated to investigate the possible origin of the observed clouds. These are shown in
323 the right panels of Figure 3, where one trajectory was calculated for each cirrus layer detected, with the
324 arrival height set to the height of top of the cirrus layer. Most of the trajectories are directed to the regions
325 of maximum accumulated precipitation (left panel), which are much closer to the site during the wet (~
326 5°) than dry (~ 10°) season. This gives further evidence that cirrus clouds observed in central Amazonia
327 are likeliest detrained anvils from tropical deep convection.
328 The backward trajectories also reveal that the high-altitude circulation is quite variable. Indeed, many
329 backward trajectories do not follow the average wind pattern and seem to point in the opposite direction
330 of precipitation, particularly during the dry season. One should note, however, that central Amazonia still
331 receives about 100 mm per month of precipitation in the dry season (reddish colors around the site, Figure
332 3) and most of it comes from mesoscale convective systems (Machado et al., 2004; Burleyson et al.,
333 2016). Hence, during the dry season, there is a mixture of locally produced and long-range transported
334 cirrus, in contrast to the wet season when there is always near-by convection.
335 The diurnal cycle of cirrus cloud frequency, shown in Figure 4, also has a close relation with the
336 convective cycle. The frequency of occurrence, for the overall period or any season, exhibits a minimum
337 between 10 and 14 hours local time (LT). Maximum values are found between 17 and 18 LT, in the late
338 afternoon, when values are slightly higher than in the morning. This diurnal variation follows the diurnal
339 cycle of convection documented in the literature (e.g. Machado et al., 2002; Silva et al., 2011, Adams et
340 al. 2013), as also shown in Figure 4 as the diurnal cycle of precipitation averaged over an area of 2° x 2°
341 centered on the experimental site. Maximum precipitation occurs between 13 and 18 LT, during both the
342 dry and the wet seasons, which coincides with the increase in cirrus frequency. In Figure 4, a smaller
343 amplitude in cirrus frequency during the wet season versus the dry season months is seen. This can be
344 reconciled by analyzing the maximum precipitation rates and the upper-altitude circulation (see Figure 3).
345 When the frequency of deep convection is greater (3 times more in the wet season) and closer to the site
346 (~5° in the wet and ~10° in the dry), the cirrus clouds, which are long-lived, presumably get more evenly
347 distributed during the day.
348 To verify that the lower cirrus cloud cover around noon was not related to a decrease in SNR and, hence,
349 a decrease in detection efficiency, we analyzed the frequency of occurrence for different cirrus types
350 (following Sassen and Cho, 1992). Opaque (COD > 0.3), thin (0.3 > COD > 0.03) and sub-visual cirrus
351 (SVC) clouds (COD < 0.03) were considered. Their diurnal variation is also shown in Figure 4. The
352 frequency of occurrence of opaque cirrus has the larger amplitude, during both dry and wet seasons.
353 During the dry (wet) season, it increases from less than 5 % (20 %) to about 30 % (50 %) in the hours
354 following the precipitation maximum, 15 h to 19 h LT. The second larger diurnal variation corresponds to
355 the occurrence frequency of thin cirrus, which decreases after the sunrise from 30 % (50 %) to 20 % (30
356 %) during the dry (wet) season, and increase again during night time, when the opaque cirrus clouds are
357 dissipating. The SVC, whose detection could be biased by lower SNR, do not show a clear diurnal cycle.

371 Hence, the diurnal cycle of the frequency of occurrence of cirrus clouds in central Amazonia is likely a

372 result of the diurnal cycles of opaque and thin cirrus, which have a sufficiently high COD to not be

373 missed by the detection algorithm.

3.2. Geometrical, optical and microphysical properties of cirrus clouds.

375 Table 2 shows column-integrated statistics of the properties of cirrus clouds during the one-year

376 observational period, also distinguished by season. Column-integrated COD varies from 0.25 ± 0.45 in

377 the dry season to 0.47 ± 0.65 in the wet season. The frequency of occurrence of opaque, thin and SVC

378 column-integrated COD is 11.8 % (31.3 %), 23.9 % (37.9 %) and 23.3 % (18.3 %) respectively in the dry

379 (wet) season. The maximum backscattering altitude does not show a seasonal cycle, and is on average

380 13.4 ± 2.0 km (or -60 ± 15 °C). The average number of simultaneous layers of cirrus present in each

381 cloudy profile is 1.4 (1.25 during the dry, and 1.62 during the wet season), and hence geometrical

382 properties, in a column-integrated sense, are not discussed.

383 As cirrus at different altitudes might have different origins or microphysical properties, it is more

384 important to analyze the statistics based on each layer detected, as shown in Table 3. The overall mean

385 value for the cloud layer base altitude is 12.9 ± 2.2 km, for the cloud layer top altitude, 14.3 ± 1.9 km, and

386 for the cloud layer geometrical thickness, 1.4 ± 1.1 km. The mean value of the cloud layer maximum

387 backscattering altitude is 13.6 ± 2.0 km. The differences between the mean values of the geometrical

388 properties in the dry and wet seasons are not statistically significant, except for the thickness, which

389 changes from 1.3 km to 1.5 km, respectively. These values are similar to those reported by Seifert et al.

390 (2007) for the Maldives (4.1 °N, 73.3 °E): 11.9 ± 1.6 km (base), 13.7 ± 1.4 km (top), 1.8 ± 1.0 km

391 (thickness), 12.8 ± 1.4 km (max. backscatter) and −58 ± 11 °C (temperature at max. backscatter). Reports

392 from subtropical regions also show similar values. Cadet et al. (2003) report for the Reunion Island (21°S,

393 55°E) cirrus cloud base and top altitudes of 11 km and 14 km, respectively. Antuña and Barja (2006)

394 report for a subtropical experimental site (Camagüey, Cuba, 21.4° N, 77.9° W) cirrus cloud base and top

395 altitudes of 11.63 km and 13.77 km, respectively. On the other hand, Sassen and Campbell (2001) show

396 mean values for midlatitude cirrus cloud base and top of 8.79 km and 11.2 km, respectively, which is

397 lower than for tropical cirrus, and an average geometrical thickness of 1.81 km. Some cirrus cloud

398 characteristics reported around the globe are shown in Table 1 for comparison.

399 The geometrical characteristics of the detected cirrus clouds were further examined by means of

400 normalized histograms. Figure 5 shows the results for cloud base and top height, thickness and cloud

401 optical depth. Histograms for the wet and dry season months reveal differences. The cloud base

402 distribution (Figure 5a) is wider during the wet season. There are relatively more cirrus layers with cloud

403 base below 12 km and above 16.5 km during the wet than during the dry season. Particularly, there is a

404 peak centered at 16.5 km during wet months, which does not exist during the dry season months. The

405 distribution of geometrical thickness (Figure 5b) shows more cirrus layers thicker than 2 km (and less

406 thinner than that) in the wet season. The normalized histogram of COD (Figure 5d) shows relatively more

407 cirrus layers with COD > 0.1 in the wet season, and more with COD < 0.1 in the dry season. The largest

408 differences, however, are seen in the cirrus cloud top altitude distribution (figure 5c). It shows two peaks

409 in the wet months, one centered at 14.25 km and second centered at 17.75 km. On the other hand, for dry

9

months, there is only one peak centered at 15.75 km. These differences suggest different cirrus types with different origins.

Comstock et al. (2002) proposed two different types of cirrus clouds at Nauru Island in the tropical western Pacific with oceanic conditions: one type (laminar thin cirrus) with cloud base altitudes above 15 km and the other (geometrically thicker and more structured cirrus) with base altitudes below this height, with different characteristics. Liu and Zipser (2005) used TRMM Precipitation Radar (PR) dataset to trace the deep convection and precipitation throughout the tropical zone, including oceans and continents. The authors showed that only 1.38 % and 0.1 % of tropical convective systems, and consequently their generated cirrus clouds, reached 14 km and 16.8 km of altitude, respectively.

Considering these previous results, we suggest that the highest peak in wet months in cloud top distribution originates from convection penetrating the tropopause, located at about 15.9-16.5 km, while the lowest peak is the ceiling of most tropical convection. The single peak observed during the dry months, in turn, originates from cirrus clouds transported by large distances. Clouds generated by convective systems can persist in the atmosphere from hours to days if they are slowly lifted (Ackerman et al., 1988; Seifert et al., 2007). Clouds that ascended and are horizontally transported by long distances are, in general, optically and geometrically thinner and found at higher altitudes in the troposphere. This also explains why the geometrical thicknesses and optical depth are lower during the dry season months.

To investigate if the higher cirrus layers were indeed geometrically and optically thinner, a more in-depth analysis of the vertical distribution was performed. Figure 6 shows two-dimensional histograms of cloud optical depth and cirrus occurrence vertical distribution for the wet season months (top) and dry season months (bottom). The right panels show the vertical distribution of the frequency of occurrence for the three cirrus categories. During the wet months, there is more dispersion (wider range of COD for a fixed altitude, and vice-versa) than in the dry months, which we speculate might be associated with the well-documented variability in the intensity of deep convection in Amazonia (Machado et al., 2002; Adams et al., 2009, 2013, 2015). Indeed, it is only during the wet season that a significant fraction of cirrus is found above 16 km height, and they have a COD ranging from 0.001 to 0.02. Moreover, while the distribution of opaque cirrus peaks at 12 km height in both seasons, thin cirrus and SVC shows a bimodal distribution only in the wet season, with the highest maxima above 14 km and 16 km respectively. This is presumably associated with the overshooting convection discussed above, which occurs mostly during the wet season (Liu and Zipser, 2005). Moreover, ice detrainment directly into the tropical tropopause layer (TTL) is one of the main mechanisms of TTL cirrus formation; the other is in-situ formation by supersaturation promoted by mesoscale uplift (Cziczo et al., 2013), which can occur above tropical convective systems (Garret et al., 2004), a very common feature of the Amazon hydrological cycle.

To investigate the role of the tropopause capping on the cirrus vertical development, its altitude was calculated from the ERA Interim dataset for the observation time of each cirrus profiles (see section 2.2 and Figures S.3a and S.3b). The tropopause mean altitudes during the wet, transition and dry periods are 16.5 ± 0.2 km, 16.3 ± 0.3 and 15.9 ± 0.4, respectively. Therefore, a non-negligible fraction of the observed cirrus during the wet and dry seasons (Figure 6) occurred likely above the tropopause. Figure 7 shows the distribution of the distance from the cloud top and bottom to the tropopause. About 7 % (19 %) of the detected cirrus clouds have their cloud base (top) above the tropopause during the wet season, and

10

464 5 % (13 %) during the dry season. Most of the cirrus cloud tops are found right below the tropopause
465 inversion, except during the wet season when they are uniformly distributed from -2 km to +0.5 km,
466 which is associated with the variability in deep convection intensity as discussed above. During the dry
467 season, on the other hand, deep convection overshooting occurs primarily north of the equator (Figure 2
468 from Liu and Zipser, 2005). These cirrus that form around the tropopause cannot last for a long time
469 (typically less than a day; Jensen et al., 1996), as they cannot be lifted above the tropopause inversion.
470 Therefore, they cannot be transported over long distances and do not reach the measurement site, hence
471 there is only one maximum near 15 km in the distribution of cloud tops, which is just below the
472 tropopause.

473 The classification of cirrus clouds following Sassen and Cho (1992) shows that 41.6 % of the cirrus
474 clouds measured in our experimental site are subvisible ($\tau < 0.03$), 37.8 % are thin cirrus ($0.03 < \tau < 0.3$)
475 and 20.5 % are opaque cirrus ($\tau > 0.3$). Table 3 shows these values for each season. SVC clouds have the
476 highest (lower) fraction during dry (wet) months. Opaque clouds have the highest (lowest) fraction during
477 wet (dry) months, which is expected, as there is a predominance of newly-generated clouds by deep
478 convection.

479 This large fraction of optically thin and subvisible cirrus clouds over Amazonia present a challenge for
480 using passive remote sensing from space, such as MODIS. As mentioned by Ackerman et al. (2010), thin
481 cirrus clouds are difficult to detect because of insufficient contrast with the surface radiance. MODIS only
482 detects cirrus with optical depth typically higher than 0.2 (Ackerman et al., 2008). Therefore, the
483 MODIS's cloud-mask does not include 71 % of cirrus clouds over Amazonia, and likewise, their
484 estimation of aerosol optical depth might be contaminated with these thin cirrus. Aerosol optical depth
485 measurements from AERONET can also be contaminated with thin cirrus clouds. Chew et al. (2011), for
486 instance, estimated that the fraction of contaminated measurements of AERONET AOD in Singapore
487 (1.5° N, 103.7° E) is about 0.034 to 0.060. The determination of the actual contamination of MODIS and
488 AERONET aerosol products for Amazonia by thin cirrus will be the subject of a forthcoming study.

489 The different types of cirrus clouds measured in central Amazonia, with different formation mechanisms,
490 optical depths and altitude ranges are expect to be composed of ice crystals of different shapes. One way
491 to gain information on the crystal habits is to compute the lidar-ratio (Sassen et al., 1989). As explained in
492 section 2, we are able to estimate the average lidar ratio for the detected cirrus cloud layers in each profile
493 using an interactive approach instead of explicitly calculating the extinction from the Raman signal,
494 which would be available only during night-time.

495 Average values are given in Table 3 for all cirrus, and for each category. A mean value of 23.9 ± 8.0 (std)
496 sr was obtained for the whole period and the variation is less than 1.5 sr for the different seasons (i.e., it
497 does not show a seasonal cycle). For opaque, thin and SV cirrus the means are 25.7 ± 6.3 sr, 22.8 ± 7.9 sr
498 and 21.6 ± 8.4 sr, respectively. Pace et al., (2003) found a mean value of lidar ratio of 19.6 sr for the
499 tropical site of Mahé, Seychelles. Seifert et al.(2007), also for tropical regions, report values close to
500 32 sr. Platt and Diley (1984) reported the value of 18.2 sr with an error of 20%. For the other latitudes,
501 examples are given in Table 1. We note, however, that the lidar ratio may vary greatly depending on the
502 altitude and composition of cirrus clouds (Goldfarb et al., 2001), but also on the correction for multiple

Henrique de Melo Jorg…, 1/2/2017 15:08
Deleted: has

Henrique de Melo Jorg…, 1/2/2017 15:08
Deleted: ed

Henrique de Melo Jorg…, 7/2/2017 14:30
Deleted: adiabatically

Henrique de Melo Jorg…, 7/2/2017 14:30
Deleted: (Jensen et al., 1996)

Henrique de Melo Jorg…, 1/2/2017 15:09
Deleted:

Henrique de Melo Jorg…, 1/2/2017 15:09
Deleted:

Henrique de Melo Jorg…, 1/2/2017 15:10
Deleted: find

Henrique de Melo Jorg…, 1/2/2017 15:10
Deleted: ,

scattering (Platt, 1981; Hogan, 2008). The latter depends on the ice crystals effective radius, and the associated uncertainty can range from 20 to 60 % (Wandinger, 1998).

Although the mean LR for all seasons and categories are similar, their statistical distribution might yet reveal differences. Figure 8 shows the histograms of lidar ratio corrected for multiple-scattering for the different seasons (top) and for the different categories (bottom). For all seasons, the most frequent lidar ratios are between 18 sr and 28 sr. There are notable differences only for different cirrus categories. The opaque cirrus distribution has a peak at 25 sr, while thin cirrus has its peak at about 21 sr, and SVC at about 15 sr, with a secondary peak at 44 sr.

As cirrus microphysical properties are expected to depend on altitude (e.g., Goldfarb et al., 2001), we examine the dependence of the lidar ratios with the cirrus cloud top temperature (Figure 9). The plots show the mean, the median, and the interquartile distance. A slight increase in the lidar ratio values from 20 sr to 28 sr for a decrease in temperature from -40 to -55 °C can be noticed during the dry period. During the wet period, the lidar ratio values are between 18 sr and 28 sr in all temperature intervals. Seifert et al. (2007) and Pace et al. (2003) both show the same temperature dependence of the lidar ratio, but with different mean values of the lidar ratio. This behavior is an indication of a slight variation in the microphysical characteristics of the observed clouds.

4. Conclusions.

One year of ground-based lidar measurements collected between July 2011 and June 2012 were used to investigate the geometrical and optical properties of cirrus clouds in central Amazonia. An algorithm was developed to search through this dataset with high vertical and temporal resolution and to automatically find clouds, calculate particle backscatter, and derive optical depth and lidar ratio. The frequency of cirrus cloud occurrence during the observation period was 73.8 %, which is higher than reported previously in the literature for other tropical regions. Cirrus frequency reached 88.1 % during the wet months (January, February, March and April), but decreased to 59.2 % during the dry months (June, July, August, and September). Analysis of high-level circulation and precipitation during the wet months indicate that near-by deep convection was likely the main source of these cirrus. Whilst during the dry period, there was a mixture of locally produced and transported clouds. Moreover, we found that the diurnal cycle of the frequency of occurrence of opaque and thin cirrus shows a minimum around 12h LT and a maximum around 18h LT, following the diurnal cycle of the precipitation for both seasons.

The geometrical and optical characteristics of cirrus clouds measured in the present study were consistent with other reports from tropical regions. The mean values were 12.9 ± 2.2 km (base), 14.3 ± 1.9 km (top), 1.4 ± 1.1 km (thickness), and 0.25 ± 0.46 (optical depth). Cirrus clouds were found at temperatures down to −90 °C and maximum backscatter altitude was 13.6 ± 2.0.

By simultaneously analyzing cloud altitude and COD, it was found that cirrus clouds observed during the dry season months are optically thinner and lower in altitude than those during the wet period. The vertical distribution of frequency of occurrence is mono-modal, and 13 % of the observed cirrus had top within the TTL. During the wet season months, there is a wider range of COD for a fixed altitude, and vice-versa, which is associated with the variability in the intensity of deep convection in Amazonia. The vertical distribution of the frequency of occurrence of the detected clouds shows a bimodal distribution

12

Henrique de Melo Jorg…, 1/2/2017 15:11
Deleted: the

Henrique de Melo Jorg…, 1/2/2017 15:11
Deleted: performed

Henrique de Melo Jorg…, 1/2/2017 15:11
Deleted: near-by

Henrique de Melo Jorg…, 1/2/2017 15:12
Deleted: advected

Henrique de Melo Jorg…, 7/2/2017 15:42
Deleted: ,

Henrique de Melo Jorg…, 7/2/2017 15:42
Deleted: and microphysical

Henrique de Melo Jorg…, 7/2/2017 15:49
Deleted: 6 % (16 %) of the observed cirrus had their base (top) above the tropopause level or in the tropical tropopause layer.

for thin and SV cirrus, and 19 % of the observed cirrus had top within the TTL, which are likely associated to slow mesoscale uplifting or to the remnants of overshooting convection.

For the first time, the lidar ratio of cirrus clouds was obtained for the Amazon region. The mean lidar ratio, corrected for multiple-scattering, was 23.6 ± 8.1 sr, in agreement with other reports from the tropical regions. The statistical distribution of lidar ratios measured during the different seasons is the same, and they also do not vary with temperature (altitude) of the clouds, indicating that these are well mixed vertically. It was observed, however, that the distributions of the lidar ratio for different cirrus categories are quite different. They are more skewed towards lower lidar ratios for smaller COD. From all cirrus clouds observed, 41.6 % were classified as subvisible (COD < 0.03), 37.8 % as thin (0.03 < COD < 0.3) and 20.5 % as opaque (COD > 0.3). During the dry months, subvisible cirrus clouds reached a maximum frequency of occurrence of 46 %, while opaque cirrus have their maximum during the wet season months (25.2 %). These values are characteristic for the region under study and somewhat different from other tropical regions. Thus, central Amazonia has a high frequency of cirrus clouds in general, and a large fraction of subvisible cirrus clouds. Therefore, the aerosol optical depth determined by Sun photometers and satellite based sensors in this region might be contaminated by the presence of these thin clouds. Future work must be conducted in order to evaluate how large this contamination might be over Amazonia.

5. Acknowledgements

6. References

Ackerman, S., Holz, R., Frey, R., and Eloranta, E.: Cloud Detection with MODIS: Part II Validation, J Atmos Oceanic Tech, 25(1073-1086), doi:DOI:10.1175/2007JTECHA1053.1, 2008.

Ackerman, S., Frey, R., Strabala, K., Liu, Y., Gumley, L., Baum, B., Menzel, P.: Discriminating Clear-Sky From Cloud With MODIS. Algorithm Theoretical Basis Document (MOD35). ATBD Version 6.1. October 2010. 2010.

602 Adams, D. K., Souza, E., and Costa, A.: Moist Convection in Amazonia: Implications for Numerical
603   Modeling (in Portuguese). Revista Brasileira de Meteorologia, 13, 168-178, 2009.

604 Adams, D. K., Gutman, S. I., Holub, K. L., and Pereira, D. S.: GNSS observations of deep convective
605   time scales in the Amazon. Geophysical Research Letters, 40, 2818-2823, 2013.

606 Adams, D. K., Fernandes, R. M. S., Holub, K. L., Gutman, S. I., Barbosa, H. M. J., Machado, L. A.T.,
607   Calheiros, A. J. P., Bennett, R. A., Kursinski, E. R., Sapucci, L. F., DeMets, C., Chagas, G. F. B.,
608   Arellano, A., Filizola, N., Amorim Rocha, A. A., Araújo Silva, R., Assunção, L. M. F., Cirino, G.
609   G., Pauliquevis, T., Portela, B. T. T., Sá, A., de Sousa, J. M., and Tanaka, L. M. S: The Amazon
610   Dense GNSS Meteorological Network: A New Approach for Examining Water Vapor and Deep
611   Convection Interactions in the Tropics. Bull. Amer. Meteor. Soc., 96, 2151–2165, 2015.

612 Antuña, J. C. and Barja, B.: Cirrus cloud optical properties measured with lidar in Camagüey, Cuba,
613   Óptica Pura y Aplicada, 39, 11–16, 2006.

614 Arraut, J.M., Nobre, C.A., Barbosa, H.M.J., Marengo J.A., and Obregon, G.: Aerial Rivers and Lakes:
615   looking at large scale moisture transport, its relation to Amazonia and to Subtropical Rainfall in
616   South America, J. Climate, 25, pp. 543-556, doi: 10.1175/2011JCLI4189.1, 2012.

617 Baars, H., Ansmann, A., Althausen, D., Engelmann, R., Heese, B., Müller, D., Artaxo, P., Paixao, M.,
618   Pauliquevis, T., and Souza, R.: Aerosol profiling with lidar in the Amazon Basin during the wet
619   and dry season, J. Geophys. Res., 117, D21201, 2012.doi:10.1029/2012JD018338, 2012.

620 Barja, B., Aroche, R.: Cirrus clouds at Camagüey, Cuba, Proceedings of the SPARC 2000, 2001.

621 Barja, B. and Antuña, J. C.: The effect of optically thin cirrus clouds on solar radiation in Camagüey,
622   Cuba, Atmos. Chem. Phys., 11, 8625–8634, doi:10.5194/acp-11-8625-2011, 2011.

623 Barbosa, H. M. J., Barja, B., Pauliquevis, T., Gouveia, D. A., Artaxo, P., Cirino, G. G., Santos, R. M. N.,
624   and Oliveira, A. B.: A permanent Raman lidar station in the Amazon: description, characterization,
625   and first results, Atmos. Meas. Tech., 7, 1745-1762, doi:10.5194/amt-7-1745-2014, 2014.

626 Boucher, O., Randall, D., Artaxo, P., Bretherton, C., Feingold, G., Forster, P., Kerminen, V.-M., Kondo,
627   Y., Liao, H., Lohmann, U., Rasch, P., Satheesh, S.K., Sherwood, S., Stevens, B., and Zhang, X.Y.:
628   Clouds and Aerosols. In: Climate Change 2013: The Physical Science Basis. Contribution of
629   Working Group I to the Fifth Assessment Report of the Intergovernmental Panel on Climate
630   Change [Stocker, T.F., D. Qin, G.-K. Plattner, M. Tignor, S.K. Allen, J. Boschung, A. Nauels, Y.
631   Xia, V. Bex and P.M. Midgley (eds.)]. Cambridge University Press, Cambridge, United Kingdom
632   and New York, NY, USA, 2013.

633 Bucholtz, A.: Rayleigh-scattering calculations for the terrestrial atmosphere, Applied Optics 34, 2765–
634   2773, 1995.

635 Burleyson, C., Z. Feng, S. Hagos, J. Fast, L. Machado, and S. Martin, Spatial Variability of the
636   Background Diurnal Cycle of Deep Convection around the GoAmazon2014/5 Field Campaign
637   Sites. *J. Appl. Meteor. Climatol.,* **55**, 1579–1598, doi: 10.1175/JAMC-D-15-0229.1, 2016

638 Campbell, J. R., Vaughan, M. A., Oo, M., Holz, R. E., Lewis, J. R., and Welton, E. J., Distinguishing
639   cirrus cloud presence in autonomous lidar measurements, Atmos. Meas. Tech., 8, 435-449,
640   doi:10.5194/amt-8-435-2015, 2015.

641 Campbell, J., S. Lolli, J. Lewis, Y. Gu, and E. Welton, Daytime Cirrus Cloud Top-of-the-Atmosphere
642   Radiative Forcing Properties at a Midlatitude Site and Their Global Consequences. J. Appl.
643   Meteor. Climatol., 55, 1667–1679, doi: 10.1175/JAMC-D-15-0217.1, 2016

644 Cadet, B., Goldfarb, L., Faduilhe, D., Baldy, S., Giraud, V., Keckhut, P., and Réchou, A., A sub-tropical
645   cirrus clouds climatology from Reunion Island (21°S, 55°E) lidar data set, Geophys. Res. Lett.,
646   30(3), 1130, doi:10.1029/2002GL016342, 2003.

647 Chen, W.; Chiang, C.; Nee, J.: Lidar ratio and depolarization ratio for cirrus clouds. Applied Optics, v.
648   41, n. 30, p. 6470 6476, 2002.

649 Chew B, Campbell J, Reid J, Giles D, Welton E, Salinas S, Liew S.: Tropical cirrus cloud contamination
650   in sun photometer data. Atmospheric Environment;45 (37):6724-6731, 2011.

651 Comstock, J. M., Ackerman, T. P., and Mace, G. G.: Ground-based lidar and radar remote sensing of
652   tropical cirrus clouds at Nauru Island: Cloud Statistics and radiative impacts, J. Geophys.
653   Res.,107, 4714, doi:10.1029/2002JD002203, 2002.

654 Cziczo, D. J., Froyd, K. D., Hoose, C., Jensen, E. J., Diao, M., Zondlo, M. A., Smith, J. B., Twohy, C. H.,
655   and Murphy, D. M.: Clarifying the dominant sources and mechanisms of cirrus cloud formation.,
656   Science, 340, 1320–1324, doi:10.1126/science.1234145, 2013.

657 Fernald, F. G., Herman, B. M. and Reagan, J. A.: Determination of aerosol height distribution by lidar,
658   Appl. Opt., 11, 482–489, 1972.

659 Fortuin, J. P. F., Becker, C. R., Fujiwara, M., Immler, F., H. M. Kelder, Scheele, M. P., and Schrems, O.,
660   Verver, G. H. L.: Origin and transport of tropical cirrus clouds observed over Paramaribo,
661   Suriname (5.8°N, 55.2°W), J. Geophys. Res., 112, D09107, doi:10.1029/2005JD006420, 2007.

662 Garrett, T. J., A. J. Heymsfield, M. J. McGill, B. A. Ridley, D. G. Baumgardner, T. P. Bui, and C. R.
663   Webster (2004), Convective generation of cirrus near the tropopause, J. Geophys. Res., 109,
664   D21203, doi:10.1029/2004JD004952.

665 Giannakaki, E., Balis, D. S., Amiridis, V., and Kazadzis, S.: Optical and geometrical characteristics of
666   cirrus clouds over a Southern European lidar station, Atmos. Chem. Phys., 7, 5519–5530,
667   doi:10.5194/acp-7-5519-2007, 2007.

668 Goldfarb, L., Keckhut, P., Chanin, M.-L., and Hauchecorne, A.: Cirrus climatological results from lidar
669   measurements at OHP (44° N, 6° E), Geophys. Res. Lett., 28, 1687–1690, 2001.

670 Hoareau, C., Keckhut, P., Noel, V., Chepfer, H., and Baray, J.-L.: A decadal cirrus clouds climatology
671   from ground-based and spaceborne lidars above the south of France (43.9° N–5.7° E), Atmos.
672   Chem. Phys., 13, 6951–6963, doi:10.5194/acp-13-6951-2013, 2013.

673 Hogan, R. J., and Kew, S. F.: A 3D stochastic cloud model for investigating the radiative properties of
674   inhomogeneous cirrus clouds. Q. J. R. Meteorol. Soc., 131, 2585-2608, 2005.

675 Hong, G., Heygster, G., Miao, J., and Kunzi, K.: Detection of tropical deep convective clouds from
676   AMSU-B water vapor channels measurements, J. Geophys. Res., 110, D05205,
677   doi:10.1029/2004JD004949, 2005.

678 Huffman, G.J., Adler, R.F., Bolvin, D.T., Gu, G., Nelkin, E.J., Bowman, K.P., Hong, Y., Stocker, E.F.,
679   and Wolff, D.B.,: The TRMM multi-satellite precipitation analysis: quasi-global, multi-year,
680   combined-sensor precipitation estimates at fine scale. J. Hydrometeorol. 8 (1), 38–55, 2007.

681 Immler, F. and Schrems, O.: LIDAR measurements of cirrus clouds in the northern and southern
682   midlatitudes during INCA (55° N, 53° S): A comparative study, Geophys. Res. Lett., 29, 1809,
683   doi:10.1029/2002GL015076, 2002a.
684 Immler, F., and Schrems, O.: Determination of tropical cirrus properties by simultaneous LIDAR and
685   radiosonde measurements, Geophys. Res. Lett., 29/23, 4, doi:10.1029/2002GL015076, 2002b.
686 International meteorological vocabulary. WMO, No. 182. TP. 91. Geneva (Secretariat of the World
687   Meteorological Organization) 1966. Pp. xvi, 276. Sw. fr. 40. Q.J.R. Meteorol. Soc., 93: 148.
688   doi:10.1002/qj.49709339524
689 Jensen, E. J., Toon, O. B., Selkirk, H. B., Spinhirne, J. D., and Schoeberl, M. R.: On the formation and
690   persistence of subvisible cirrus clouds near the tropical tropopause, J. Geophys. Res., 101(D16),
691   21361–21375, doi:10.1029/95JD03575, 1996.
692 Khvorostyanov, V. I., and Sassen, K.: Microphysical processes in cirrus and their impact on radiation A
693   Mesoscale Modeling Perspective, in Cirrus ed D Lynch, K Sassen, D O C Starr and G Stephens
694   (Oxford: Oxford University Press) pp 397–432, 2002.
695 Kienast-Sjögren, E., Rolf, C., Seifert, P., Krieger, U. K., Luo, B. P., Krämer, M., and Peter, T.,
696   Climatological and radiative properties of midlatitude cirrus cloud derived by automatic evaluation
697   of lidar measurements, Atmos. Chem. Phys., 16, 7605-7621, doi:10.5194/acp-16-7605-2016,
698   2016.
699 Kim, Y., Kim, S.-W., Kim, M.-H. and Yoon, S.-C.: Geometric and optical properties of cirrus clouds
700   inferred from three-year ground-based lidar and CALIOP measurements over Seoul, Korea,
701   Atmospheric Research, 139, 27-35, 2014.
702 Klett, J.D.: Stable analytical inversion solution for processing lidar returns. Appl. Opt. 20(2), 211–220,
703   1981.
704 Krämer, M., Rolf, C., Luebke, A., Afchine, A., Spelten, N., Costa, A., Meyer, J., Zöger, M., Smith, J.,
705   Herman, R. L., Buchholz, B., Ebert, V., Baumgardner, D., Borrmann, S., Klingebiel, M., and
706   Avallone, L.: A microphysics guide to cirrus clouds – Part 1: Cirrus types, Atmos. Chem. Phys.,
707   16, 3463-3483, doi:10.5194/acp-16-3463-2016, 2016a.
708 Martina Krämer, Armin Afchine, Linnea Avallone, Darrel Baumgardner, Stephan Borrmann, Bernhard
709   Buchholz, Anja Costa, Volker Ebert, David Fahey, Robert Herman, Eric Jensen, Marcus
710   Klingebiel, P. Lawson S. Woods, Anna Luebke, Jessica Meyer, Christian Rolf, A. Rollins, T.
711   Thornberry, Jessica Smith, Nicole Spelten, Martin Zöger, Microphysical properties of cirrus
712   clouds between 75N and 25S derived from extensive airborne in-situ observations, In.: XVII
713   International Conference on Clouds & Precipitation, Manchester, 25-29 July, 2016b.
714 Lakkis, G.S., Lavorato, M., and Canziani, O.P.: Monitoring cirrus clouds with lidar in the Southern
715   Hemisphere: a local study over Buenos Aires. 1. Tropopause heights. Atmos. Res. 92 (1), 18–26,
716   2009.
717 Lin, L., Fu, Q., Zhang, H., Su, J., Yang, Q., and Sun, Z.: Upward mass fluxes in tropical upper
718   troposphere and lower stratosphere derived from radiative transfer calculations, J. Quant.
719   Spectrosc. Radiat. Transfer, 117, 114–122, 2013.

720 Liou, K. N.: Influence of cirrus clouds on weather and climate processes: A global perspective. Mon.
721   Wea. Rev., 114, 1167–1199, 1986.

722 Liu, C., and Zipser, E. J., Global distribution of convection penetrating the tropical tropopause, J.
723   Geophys. Res., 110, D23104, doi:10.1029/2005JD006063, 2005

724 Liu, C., and Zipser, E. J.: Implications of the day versus night differences of water vapor, carbon
725   monoxide, and thin cloud observations near the tropical tropopause, J. Geophys. Res., 114,
726   D09303, doi:10.1029/2008JD011524, 2009.

727 Lynch, D. K., Sassen, K., Starr, D. O., and Stephens, G.: Cirrus. Oxford University Press, 480 pp., 2002.

728 Mace, G. G., R. Marchand, Q. Zhang, and G. Stephens, Global hydrometeor occurrence as observed by
729   CloudSat: Initial observations from summer 2006, Geophys. Res. Lett., 34, L09808,
730   doi:10.1029/2006GL029017, 2007.

731 Machado, L.A.T., Laurent, H., and Lima, A.A.: Diurnal march of the convection observed during
732   TRMM-WETAMC/LBA, J. Geophys. Res., 107(D20), 8064, doi:10.1029/2001JD000338, 2002.

733 Machado, L.A.T.; Laurent, H.; Dessay, N.; Miranda, I.: Seasonal and diurnal variability of convection
734   over the Amazonia - A comparison of different vegetation types and large scale forcing.
735   Theoretical and Applied Climatology, 78, 61-77, doi: 10.1007/s00704-004-0044-9. 2004.

736 Machado, L.A.T., Silva Dias, M.A.F., Morales, C., Fisch, G., Vila,D., Albrecht, R., Goodman, S.J.,
737   Calheiros, A.J.P., Biscaro, T., Kummerow, C.,Cohen, J., Fitzjarrald, D., Nascimento, E.L.,
738   Sakamoto, M.S., Cunningham, C., Chaboureau, J. –P., Petersen, W.A., Adams, D.K., Baldini, L.,
739   Angelis, C.F., Sapucci, L.F., Salio, P., Barbosa, H.M.J., Landulfo, E., Souza, R.A.F., Blakeslee,
740   R.J., Bailey, J., Freitas, S., Lima, W.F.A., Tokay, A.: THE CHUVA PROJECT: how does
741   convection vary across Brazil? Bull. Am. Meteor. Soc., 1365–1380, doi:10.1175/BAMS-d-13-
742   00084.1, 2014.

743 Martin, S. T., Artaxo, P., Machado, L. A. T., Manzi, A. O., Souza, R. A. F., Schumacher, C., Wang, J.,
744   Andreae, M. O., Barbosa, H. M. J., Fan, J., Fisch, G., Goldstein, A. H., Guenther, A., Jimenez, J.
745   L., Pöschl, U., Silva Dias, M. A., Smith, J. N., and Wendisch, M.: Introduction: Observations and
746   Modeling of the Green Ocean Amazon (GoAmazon2014/5), Atmos. Chem. Phys., 16, 4785-4797,
747   doi:10.5194/acp-16-4785-2016, 2016.

748 McCalla, C., 1981: Objective Determination of the Tropopause Using WMO Operational Definitions,
749   Office Note 246, U.S. Department of Commerce, NOAA, NWS, NMC, 18pp, October 1981.

750 Nazaryan, H., McCormick, M. P., and Menzel, W. P.: Global characterization of cirrus clouds using
751   CALIPSO data, J. Geophys. Res., 113, D16211, doi:10.1029/2007JD009481, 2008.

752 Pace, G., Cacciani, M., di Sarra, A., Fiocco, G., and Fuà, D.: Lidar observations of equatorial cirrus
753   clouds at Mahé Seychelles, J. Geophys. Res., 108(D8), 4236, doi:10.1029/2002JD002710, 2003.

754 Pandit, A. K., Gadhavi, H. S., Venkat Ratnam, M., Raghunath, K., Rao, S. V. B., and Jayaraman, A,:
755   Long-term trend analysis and climatology of tropical cirrus clouds using 16 years of lidar data set
756   over Southern India. Atmos. Chem. Phys., 15, 13833–13848, doi:10.5194/acp-15-13833-2015,
757   2015

758 Platt, C. M. R., Remote sounding of high clouds. III: Monte Carlo calculations of multiple scattered lidar
759   returns. J. Atmos. Sci., 38, 156–167, 1981

17

760 Randel, W. J. and Jensen, E. J.: Physical processes in the tropical tropopause layer and their roles in a
761   changing climate, Nat. Geosci, 6, 169–176, doi:10.1038/ngeo1733, 2013.

762 Sasano Y., and Nakane H.: Significance of the extinction/backscatter ratio and the boundary value term in
763   the solution for the two-component lidar equation", Appl. Opt., vol. 23, 11–13, 1984.

764 Sassen, K., and B. S. Cho, B. S., Subvisual/thin cirrus dataset for satellite verification and climatological
765   research, *J. Appl. Meteorol.*, 31, 1275–1285, 1992

766 Sassen, K., Starr, D. O'C., and Uttal, T.: Mesoscale and Microscale Structure of Cirrus Clouds: Three
767   Case Studies, J of the Atmos. Sci. 46:3, 371-396, 1989.

768 Sassen, K. and Campbell, J. R.: A midlatitude cirrus cloud climatology from the facility for atmospheric
769   remote sensing. Part I: Macrophysical and synoptic properties, J. Atmos. Sci., 58, 481–496, 2001.

770 Sassen, K.: Cirrus Clouds. A Modern Perspective, In Cirrus D. Lynch, K. Sassen, D. O´C Starr, and G.
771   Stephens Eds., Oxford University Press, 136-146, 2002.

772 Sassen, K., Wang, Z., and Liu, D.: Global distribution of cirrus clouds from CloudSat/Cloud-Aerosol
773   Lidar and Infrared Pathfinder Satellite Observations (CALIPSO) measurements, J. Geophys. Res.,
774   113, D00A12, doi:10.1029/2008JD009972, 2008.

775 Sassen, K., Wang, Z., and Liu, D.: Cirrus clouds and deep convection in the tropics: Insights from
776   CALIPSO and CloudSat, J. Geophys. Res., 114, D00H06, doi:10.1029/2009JD011916, 2009.

777 Seifert, P.; Ansmann, A.; Muâller, D.; Wandinger, U.; Althausen, D.; Heymsfield, A. J.; Massie, S. T.;
778   Schmitt, C.: Cirrus optical properties observed with lidar, radiosonde and satellite over the tropical
779   indian ocean during the aerosol-polluted northeast and clean maritime southwest monsoon. J.
780   Geophys. Res., v. 112, p. D17205, 2007.

781 Silva, V. B. S., Kousky, V. E., and Higgins, R. W.: Daily Precipitation Statistics for South America: An
782   Intercomparison between NCEP Reanalyses and Observations. J. Hydrometeorol., 12, 101-117.
783   DOI: 10.1175/2010JHM1303.1, 2011.

784 Stein, A.F., Draxler, R.R, Rolph, G.D., Stunder, B.J.B., Cohen, M.D., and Ngan, F., NOAA's HYSPLIT
785   atmospheric transport and dispersion modeling system, Bull. Amer. Meteor. Soc., 96, 2059-2077,
786   doi:10.1175/BAMS-D-14-00110.1, 2015

787 Stubenrauch, C. J., Chédin, A., Rädel, G., Scott, N. A., and Serrar, S.: Cloud Properties and Their
788   Seasonal and Diurnal Variability from TOVS Path-B. J. Climate, 19, 5531–5553, 2006.

789 Tanaka, L. M. d. S., Satyamurty, P., and Machado, L. A. T.: Diurnal variation of precipitation in central
790   Amazon Basin. Int. J. Climatol. 34, 3574–3584, DOI: 10.1002/joc.3929, 2014.

791 Thorsen, T. J., Qiang, F., and Comstock, J. M.: Comparison of the CALIPSO satellite and ground-based
792   observations of cirrus clouds at the ARM TWP sites, J. Geophys. Res., 116, D21203,
793   doi:10.1029/2011JD015970, 2011.

794 Thorsen, T. and Q. Fu, Automated Retrieval of Cloud and Aerosol Properties from the ARM Raman
795   Lidar. Part II: Extinction. J. Atmos. Oceanic Technol., 32, 1999–2023, doi: 10.1175/JTECH-D-14-
796   00178.1, 2015.

797 Wandinger, U., Multiple-scattering influence on extinction- and backscatter-coefficient measurements
798   with Raman and high-spectral-resolution lidars, Appl. Optics, 37, 417–427, 1998.

18

799   Wang, T., and Dessler, A. E.: Analysis of cirrus in the tropical tropopause layer from CALIPSO and MLS
800   data: A water perspective, J. Geophys. Res., 117, D04211, doi:10.1029/2011JD016442, 2012.

801   Wendisch, M., et al.: The ACRIDICON–CHUVA campaign: Studying tropical deep convective clouds
802   and precipitation over Amazonia using the new German research aircraft HALO. Bull. Am. Met.
803   Soc., accepted, doi:10.1175/BAMS-D-14-00255.1, 2016

804   Westbrook, C. D., Illingworth, A. J., O'Connor, E. J. and Hogan, R. J., Doppler lidar measurements of
805   oriented planar ice crystals falling from supercooled and glaciated layer clouds. Q.J.R. Meteorol.
806   Soc., 136: 260–276, 2010.

807   Wylie, D. P., Jackson, D. L., Menzel, W. P., andBates, J. J.: Trends in global cloud cover in two decades
808   of HIRS observations. J. Climate, 18, 3021–3031, 2005.

809   Yang, P., Hong, G., Dessler, A. E., Ou, S. C., Liou, K. N., Minnis, P., and Hashvardhan,: Contrails and
810   induced cirrus: Optics and radiation. Bull. Amer. Meteor. Soc., 91, 473–478, 2010a.

811   Yang, Q., Fu, Q., and Hu, Y.: Radiative impacts of clouds in the tropical tropopause layer, J. Geophys.
812   Res., 115, D00H12, doi:10.1029/2009JD012393, 2010b.

813   Young, S.: Analysis of lidar backscatter profiles in optically thin cirrus, Appl. Opt., 34, 7019–7031, 1995.

814

19

Tables:

Table 1. Summary of some recent cirrus cloud studies based on at least a few months of ground-based lidar observations in the tropics and mid-latitudes. The first columns show the period of study and laser wavelength (nm) for each site location, for which more than one study might be available. The cirrus characteristics are those reported by the different authors, which might include: base and top height (km), thickness (km), base and top temperature (°C), frequency of occurrence (%) and lidar-ratio (sr).

Measurement site	Location	Period of study	Wavelength [nm]	Average values								
				Height [km]			Temp. [°C]		Frequency [%]		LR[sr]	
				Base	Top	Thick.	Base	Top	SVC	Thin		
Salt Lake City, Utah, USA	40.8°N 111.8°W	1986 to 1996	694	8.8	11.2	1.8	−34.4	−53.9	50	-		Sassen and Campbell (2001)
Haute Provence, France	43.9°N 5.7°E	1997 to 2007	532/1064	9.3	10.7	1.4			38		18.2	Goldfarb et al. (2001) Hoareau et al. (2013)
Thessaloniki, Greece	40.6°N 22.9°E	2000 to 2006	355/532	8.6	11.7	2.7	−38	−65		57	30	Giannakaki et al. (2007)
Seoul, South Korea	37°N, 127°E	2006 to 2009	532/1064	8.8	10.6						20	Kim et al. (2009)
Buenos Aires, Argentina	34.6 °S, 58.5 °W	2001 to 2005	532	9.6	11.8	2.4		−64.5				Lakkis et al.(2008)
Reunion Island	21°S, 55°E	1996 to 2001	532	11	14				65		18.3	Cadet et al. (2003)
Camagüey, Cuba	21.4° N, 77.9° W	1993 to 1998	532	11.6	13.8				25		10	Antuña and Barja, (2006)
Gadanki, India	13.5 N, 79.2 E	1998 to 2013	532	13.0	15.3	2.3		−65	52	36	25	Pandit et al., (2015)
Hulule, Maldives	4.1°N, 73.3°E	1999, 2000	532	11.9	13.7	1.8	−50	−65	15	49	32	Seifert et al. (2007)
Mahé, Seychelles	4.4 °S, 55.3 °E	Feb-Mar 1999	532			0.2-2.0					19	Pace et al., (2003)
Nauru Island	0.5 °S, 166.9 °E	Apr-Nov 1999	532	~14	~16							Comstock et al. (2002)

20

Table 2. Summary of column-integrated statistics for the total time of observation, as well as for the wet, transition and dry seasons. Frequency of occurrence is calculated using a conditional sampling to avoid biases (session 2.4). Mean cirrus cloud properties and standard deviation of the sample (in parenthesis) are shown. The standard deviations of the mean were calculated and used to determine if seasonal differences (wet-dry) of the mean values are statistically significant to the 95% confidence level (indicated as *) using a 2-sample t-test. Geometrical properties are not given because most cloud profiles have more than one layer of cirrus. Lidar ratio is calculated as a column average.

	Total	Wet	Transition	Dry
Observation time [%] [a]	37.4	41.5	21.9	48.9
N. prof. measured [b]	36844	13828	7423	15593
N. prof. used in analysis [c]	16025	3458	2099	10468
N. prof. discarded for apparent top [d]	476	223	148	105
Frequency of Occurrence [%]*	73.8	88.1	74.2	59.2
N. prof. w/ cirrus	11252	3145	1706	6397
Frequency of Occurrence, Opaque [%]*	22.6	31.3	24.6	11.8
N. prof. w/ cirrus, Opaque	3327	1316	610	1401
Frequency of Occurrence, Thin [%]*	32.8	37.9	36.5	23.9
N. prof. w/ cirrus, Thin	4577	1224	798	2555
Frequency of Occurrence, SVC [%]*	18.3	18.7	13.0	23.3
N. prof. w/ cirrus, SVC	3322	603	296	2423
Cloud Optical Depth*	0.35 (0.55)	0.47 (0.65)	0.40 (0.57)	0.25 (0.45)
Max Backscatter Altitude [km]*	13.4 (2.0)	13.4 (2.2)	13.3 (2.2)	13.6 (1.7)
Temperature Max. Back. Alt. [°C]*	-60 (15)	-60 (16)	-59 (17)	-62 (13)
Lidar Ratio [sr]* [e]	23.6 (8.1)	22.8 (8.0)	22.8 (7.8)	24.6 (7.7)
Num. of cirrus layers per cloud prof.	1.41 (0.63)	1.62 (0.77)	1.61 (0.67)	1.25 (0.48)

[a] Fraction of observation time to total possible time (21h per day)
[b] Total number of profiles measured, i.e. not screened for low clouds or precipitation
[c] Refers to the number of 5-min profiles with high enough SNR (section 2.4)
[d] Number of profiles with apparent cirrus top, considering only good profiles
[e] All layers in the same profile share the same average LR

Table 3. Summary of layer-statistics for the total time of observation, as well as for the wet, transition and dry seasons. Mean cirrus cloud properties and standard deviation of the sample (in parenthesis) are shown. The standard deviations of the mean were calculated and used to determine if seasonal differences (wet-dry) are statistically significant to the 95% confidence level (indicated as *) using a 2-sample t-test. Lidar ratio is calculated as a column average.

All Layers	Total	Wet	Transition	Dry
Num. of cirrus layers	15824	5096	2739	7989
Base Altitude [km]*	12.9 (2.2)	12.8 (2.4)	12.6 (2.3)	13.0 (1.9)
Top Altitude [km]	14.3 (1.9)	14.3 (2.0)	14.1 (2.0)	14.3 (1.6)
Thickness [km]*	1.4 (1.1)	1.5 (1.2)	1.5 (1.1)	1.3 (1.0)
Cloud Optical Depth*	0.25 (0.46)	0.30 (0.52)	0.26 (0.47)	0.20 (0.40)
Max Backscatter Altitude [km]	13.6 (2.0)	13.7 (2.3)	13.5 (2.2)	13.6 (1.8)
Lidar Ratio [sr]*	23.3 (8.0)	22.6 (8.1)	22.8 (7.9)	24.4 (7.9)
Relative freq. opaque cirrus [%]*	20.5	25.2	21.0	17.4
Relative freq. thin cirrus [%]	37.8	37.0	43.2	36.5
Relative freq. SVC [%]*	41.6	37.8	35.8	46.0
Base above the tropopause [%]*	5.9	6.9	5.5	5.3
Top above the tropopause [%]*	15.7	18.7	16.1	12.9
Opaque Layers				
Num. of opaque layers	3251	1283	574	1394
Base Altitude [km]*	10.7 (1.5)	10.6 (1.6)	10.4 (1.5)	10.8 (1.2)
Top Altitude [km]	13.4 (1.6)	13.5 (1.7)	13.1 (1.6)	13.6 (1.4)
Thickness [km]*	2.76 (1.02)	2.84 (1.07)	2.65 (1.04)	2.73 (0.94)
Cloud Optical Depth*	0.93 (0.64)	1.00 (0.66)	0.90 (0.66)	0.86 (0.59)
Max Backscatter Altitude [km]	12.0 (1.7)	12.1 (1.9)	11.6 (1.7)	12.1 (1.5)
Lidar Ratio [sr]*	25.7 (6.3)	26.0 (6.7)	25.8 (6.6)	25.3 (5.7)
Thin Layers				
Num. of thin layers	5985	1888	1183	2914
Base Altitude [km]*	12.9 (1.7)	13.1 (1.9)	12.9 (1.8)	12.8 (1.4)
Top Altitude [km]*	14.4 (1.7)	14.6 (2.0)	14.4 (1.8)	14.3 (1.4)
Thickness [km]*	1.46 (0.78)	1.42 (0.82)	1.49 (0.78)	1.47 (0.74)
Cloud Optical Depth	0.12 (0.07)	0.12 (0.07)	0.12 (0.07)	0.11 (0.07)
Max Backscatter Altitude [km]*	13.7 (1.7)	13.9 (1.9)	13.7 (1.9)	13.5 (1.5)
Lidar Ratio [sr]*	22.8 (7.9)	21.8 (7.7)	21.6 (7.4)	24.3 (8.1)
SVC Layers				
Num. of SVC layers	6581	1924	980	3677
Base Altitude [km]*	14.4 (1.9)	14.7 (2.1)	14.4 (2.1)	14.2 (1.6)
Top Altitude [km]*	14.9 (1.9)	15.2 (2.1)	15.0 (2.1)	14.7 (1.6)
Thickness [km]	0.51 (0.37)	0.50 (0.38)	0.53 (0.38)	0.51 (0.36)
Cloud Optical Depth	0.011 (0.008)	0.011 (0.008)	0.012 (0.009)	0.011 (0.008)
Max Backscatter Altitude [km]*	14.6 (1.9)	14.9 (2.1)	14.7 (2.1)	14.4 (1.6)
Lidar Ratio [sr]*	21.6 (8.4)	19.9 (7.6)	21.5 (8.1)	23.5 (9.0)

22

Figures:

Figure 1. Satellite-based map (Google Earth) showing the location of the lidar site (ACONVEX T0e, 2.89°S 59.97°W), 30 km upwind (north) from downtown Manaus-AM, Brazil.
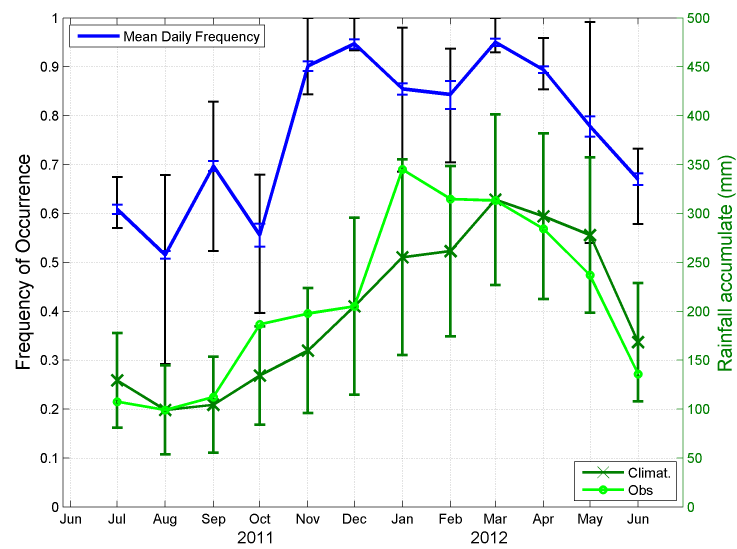
Figure 2. Monthly frequency of occurrence of cirrus clouds from July 2011 to June 2012 (blue line) with the associated statistical error (black). Accumulated (light green) and climatological (dark green) rainfall, shown on the right axis, were obtained from the TRMM 3B42 version 7 dataset averaged over an area of 10°x10°.
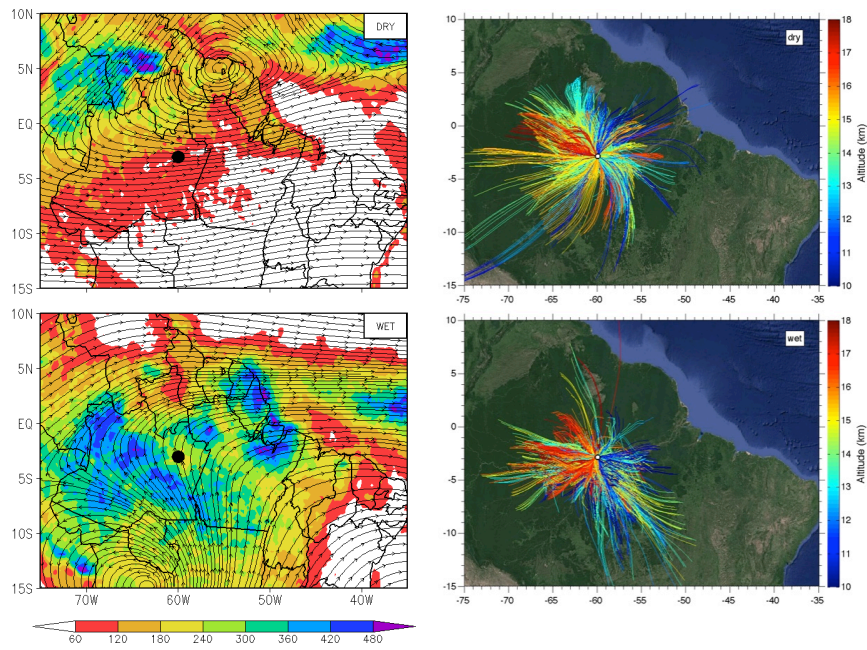
Figure 3. Left panels show mean precipitation (colors, mm month^{-1}) from the TRMM 3B42 version 7 and mean wind field (vectors, m/s) at 150 hPa (~ 14.3 km) from ECMWF ERA Interim reanalysis. Right panels show 24 h back trajectories of air masses arriving at the site at the time and altitude that cirrus layers were detected. Results are shown separately for the dry (JJAS, top) and wet months (JFMA, bottom). Backward trajectories were computed using HYSPLIT model with 0.5^{o} resolution winds from GDAS/NOAA. The experimental site location is indicated in all panels with a circle.
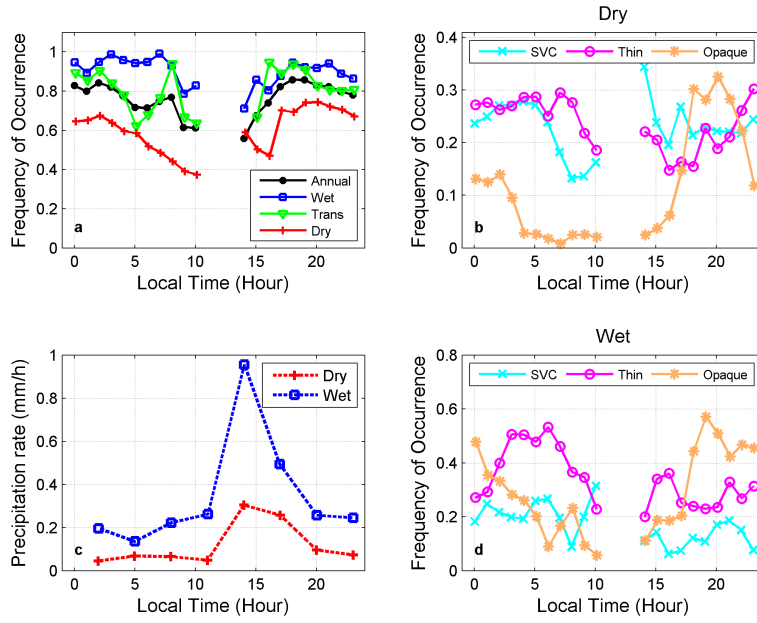
Figure 4. Panel (a) shows the daily cycles of the hourly frequency of occurrence of cirrus clouds for the annual, wet, transition and dry periods. The same is shown for SVC, thin and opaque cirrus clouds during the dry (b) and wet (d) seasons. Mean observed precipitation rate (mm/h) from TRMM version 7 over an area of 2° × 2° centered on the site, for the dry and wet periods, is given in panel (c).
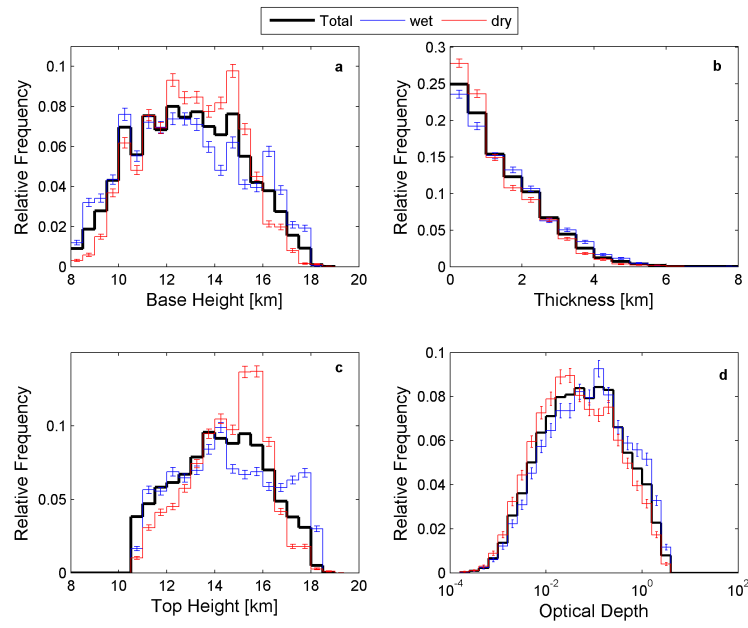
Figure 5. Panels show the normalized histograms of (a) cirrus cloud base, (b) cloud geometrical thickness, (c) cirrus cloud top, and (d) optical depth, for the overall period (black), wet season (JFMA, red) and dry season (JJAS, blue). Error bars indicate the counting statistics uncertainty.
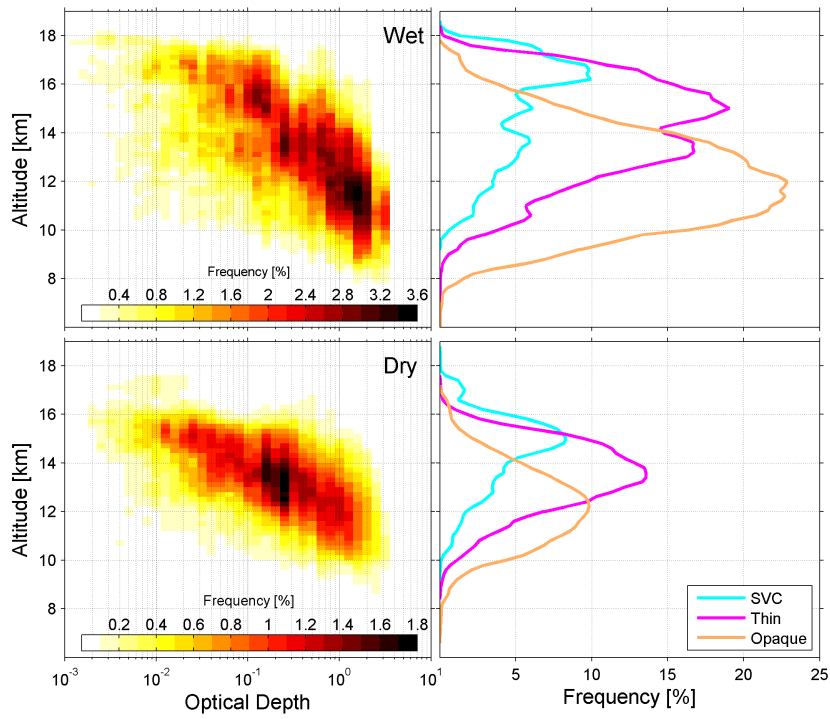
Figure 6. Two-dimensional histograms of cirrus frequency of occurrence with altitude as a function of optical depth during the wet (top) and dry (bottom) season months are shown on the left. The same is shown on the right but integrated for SVC, thin and opaque cirrus clouds optical depths.
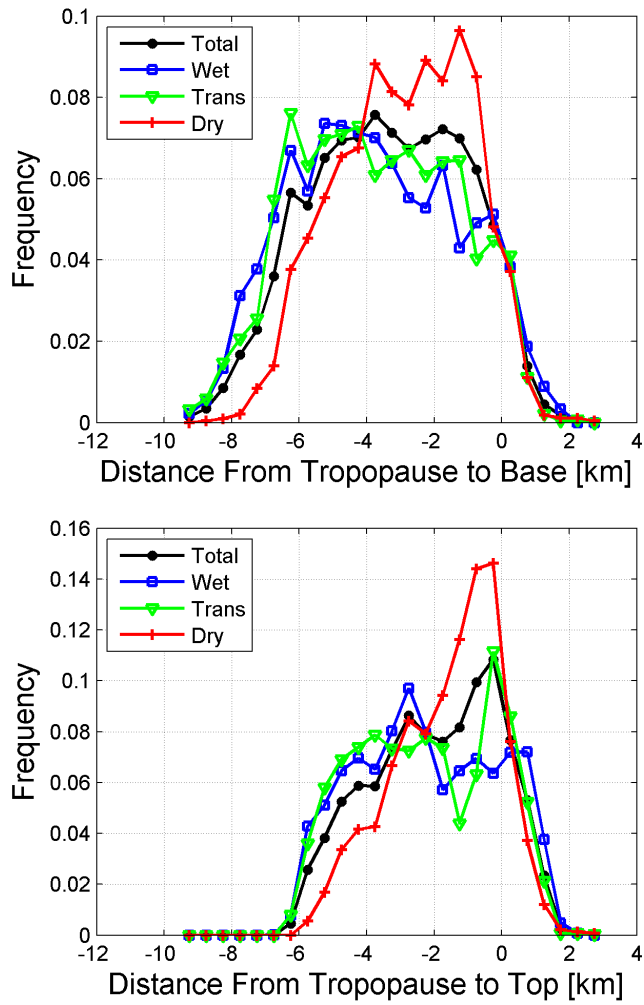
Figure 7. Normalized histograms of the distance of the tropopause to the cirrus base and top are shown for overall period (black) and each season (colors). Negative values mean that clouds are below tropopause. The average tropopause altitude was 16.2±0.4 km.
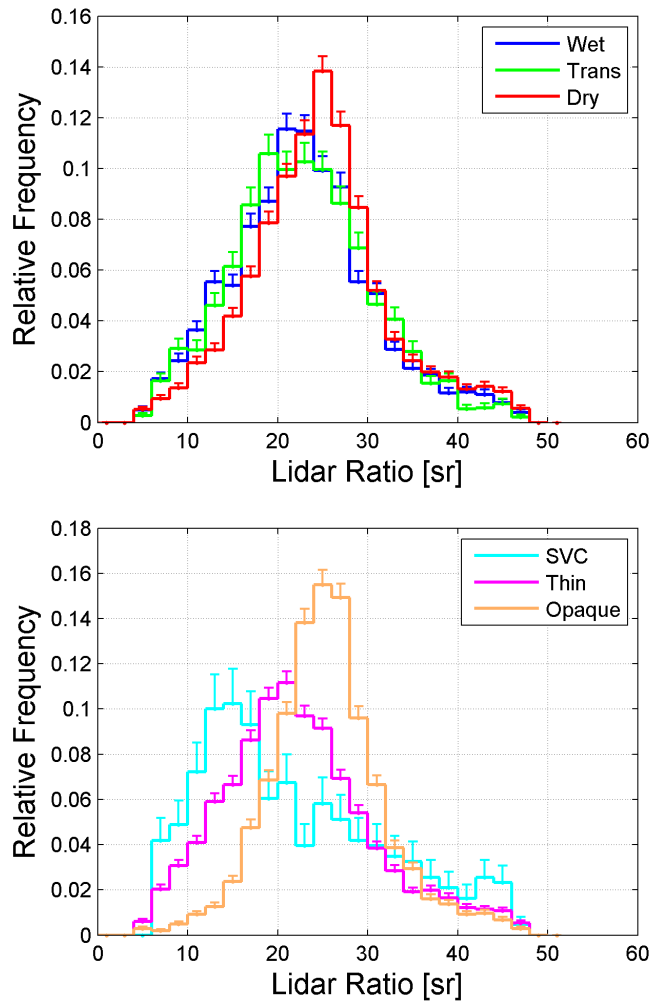
Figure 8. Normalized histograms of the lidar ratio, already corrected for multiple-scattering, for the different seasons (top) and for SVC, thin and opaque cirrus (bottom) are shown. Error bars indicate the counting statistics uncertainty.
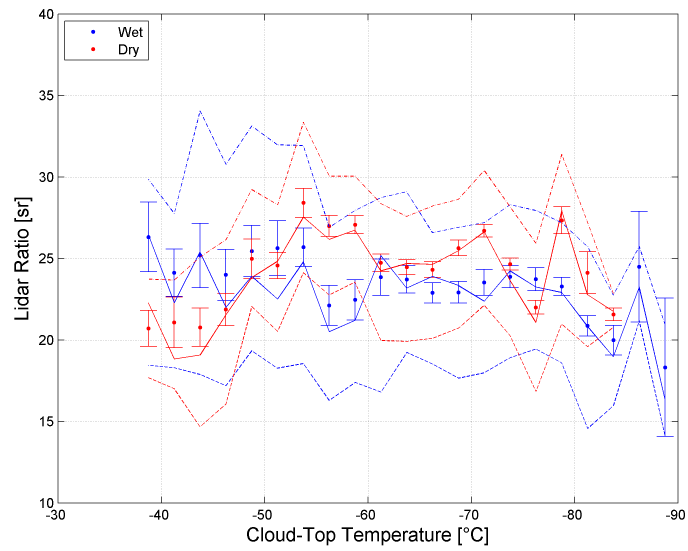
Figure 9. Dependence of the corrected lidar ratio with cloud-top temperature is shown for the wet (blue) and dry (red) seasons. The markers give mean and standard deviation of the mean. The continuous and dashed lines give median and interquartile distance. Temperature is divided in 2.5 °C intervals.